# Viscous flows in two dimensions

David Bensimon,* Leo P. Kadanoff, Shoudan Liang,† Boris I. Shraiman,* and Chao Tang‡

*The James Franck Institute, The University of Chicago, 5640 South Ellis Avenue, Chicago, Illinois 60637*

This review is an expository treatment of the displacement of one fluid by another in a two-dimensional geometry (a Hele-Shaw cell). The Saffman-Taylor equations modeling this system are discussed. They are simulated by random-walk techniques and studied by methods from complex analysis. The stability of the generated patterns (fingers) is studied by a WKB approximation and by complex analytic techniques. The primary conclusions reached are that (a) the fingers are linearly stable even at the highest velocities, (b) they are nonlinearly unstable against noise or an external perturbation, the critical amplitude for the noise being an exponential function of a power of the velocity for high velocities, (c) such exponentials seem to dominate high-velocity behavior, as can be seen from a WKB analysis, and (d) the results of the Saffman-Taylor equations disagree with experiments, apparently because they leave out film-flow phenomena.

## CONTENTS



## INTRODUCTION

This paper is an expository treatment of recent work on the stability of hydrodynamic flow patterns in two-dimensional or almost two-dimensional geometries. The basic problem is understanding the nature of the instabilities that might arise when a more viscous fluid is displaced by a less viscous one. In addition, one wants to know how surface tension can restore the stability of nontrivial flow patterns.

This paper is intended to be expository. Hence, there is an emphasis upon those parts of the field that we feel best qualified to explain, and indeed upon our own work.

In the first section, we describe the physical situation, restate the description in terms of partial differential equations, and summarize our state of knowledge about the solutions to the equations and the physical phenomena that arise. The second section relates the viscous-flow problem to a much-studied theoretical model, diffusion-limited aggregation (DLA). In these and other two-dimensional problems one can often make considerable progress by using calculational methods based upon analytic functions of complex variables. Section III describes how these methods can be used to obtain exact solutions for zero-surface tension, while Sec. IV sets up the interface equations for nonzero-surface tension. Finally, the fifth section uses complex-variable methods and WKB analysis to describe the stabilization of fingerlike flow patterns.

The case we shall consider has the simplest possible geometry. Following Hele-Shaw (1898), we consider the displacement of a more viscous fluid by a less viscous one in the very narrow gap between two parallel plates. If any fluid mechanics problem is likely to be accessible to theory and to direct comparison of theory and experiment it should be this one. The flow is almost two-dimensional potential flow. The basic partial differential equation is Laplace's equation. Despite this apparent simplicity, this problem has not been fully elucidated to this day. The basic difficulty involves the prediction of the motion of the free boundary separating two fluids. For large values of the surface tension, after a while the less viscous fluid arranges itself in a simple stable finger. In this review, we describe the recent theoretical work that shows how the finger arises and why it is stable.

However, as the surface tension gets smaller—or equivalently as the fluid velocity increases—the experiments and the simulations increasingly tend to show an unstable or chaotic pattern for the interface. In some sense, this instability is the simplest form of fluid "chaos" or (if you are willing to use the word loosely) "turbulence." Recent work, reported here, has helped us gain

*Present address: AT&T Bell Labs, Murray Hill, NJ 07974.
†Present address: Dept. of Physics, Princeton Univ., Princeton, NJ 08544.
‡Present address: Brookhaven National Laboratory, Upton, NY 11973.

a bit of understanding of this chaos. We are beginning to see how just a bit of surface tension can have a profound effect upon the evolution of the interface between two viscous fluids in a Hele-Shaw cell. As we report here, this "singular perturbation" problem is not completely understood. However, we expect that as it becomes more fully elucidated one will begin to understand more exactly how the patterns form in this relatively simple hydrodynamic system.

One additional motivation for studying this problem is that there is a long list of other apparently similar problems involving the motion of free interfaces, including directional solidification, dendritic formation, electrodeposition, dielectric breakdown, and "two-dimensional" flows in porous media. Ideas that are applicable to Hele-Shaw cells are very likely also to increase our understanding of the mathematics and physics of these other problems. In particular, some of the patterns formed in these other cases might well be understood as examples of other types of singular perturbations upon one basic, but very unstable, situation: the zero-surface-tension limit of viscous flows in a Hele-Shaw cell.

## I. THE SAFFMAN-TAYLOR PROBLEM. WHERE DO WE STAND?

### A. Introduction: phenomenology and the basic equations

The formation and evolution of dynamical structures constitute one of the most exciting areas of nonlinear phenomenology. Such pattern formation problems are common in hydrodynamic systems. Perhaps the best studied ones involve the patterns formed by the interface between two phases: a solid and a fluid, or two fluids. In turn, one of the simplest problems of this class is the Saffman-Taylor (1958) problem in which two fluids move in the narrow space between two plates. This geometry is called a Hele-Shaw cell (Hele-Shaw, 1898; see Fig. 1). When the plate separation $b$ is very small, the problem is effectively two dimensional. If we call the coordinates perpendicular to the plates $z$, and the other two $x$ and $y$, we can specify the problem by the two components of the velocity, $v_x$ and $v_y$, the pressure $P(x,y)$, and a two-component vector $\gamma(s)$, which sweeps out the position of the interface as $s$ is varied.

The basic equations involved are very simple. In each fluid, the average velocity parallel to the plates is proportional to a local force (Saffman and Taylor, 1958)

$$\mathbf{v}(x,y) = -K_i[\nabla P(x,y) - \rho_i \mathbf{g}] \ . \tag{1.1}$$

Here $i=1,2$ labels the different fluids, $\rho_i$ is the density, and the constant $K_i$ is given in terms of the fluid viscosity $\mu_i$ and the plate spacing $b$ as

$$K_i = \frac{b^2}{12\mu_i} \ , \tag{1.2}$$

while $\mathbf{g}$ is the component of the gravitational acceleration parallel to the plates. Equations (1.1) and (1.2) constitute the Darcy approximation. They are derived in a trivial way from the Navier-Stokes equation by considering a parabolic flow profile parallel to the plates with a velocity that vanishes at both plates. Then $\mathbf{v}$ is the average over the perpendicular direction of the actual velocity.

The remaining equations are easy to write down. Assume that the fluids are incompressible, so that the divergence of the velocity vanishes. Then, in each fluid

$$\nabla^2 P = 0 \ . \tag{1.3}$$

Continuity also implies a boundary condition that, at the interface, the normal components of the velocity be equal to each other and to the speed of the interface

$$v_n = -K_1(\nabla P_1)_n = -K_2(\nabla P_2)_n \ , \tag{1.4}$$

where the gradients are evaluated at the points $\gamma(s)$.

One more boundary condition is needed to give the jump in pressure across the interface. Theorists working on this problem often choose to take the pressure jump to be the surface tension $T$ times the curvature $\kappa$ observed in the $xy$ plane, i.e.,

$$\Delta P = T\kappa \ . \tag{1.5a}$$

This formula would follow if the classical Gibbs-Thomson equations for the pressure jump were really applicable. This, in turn, would be true if the Hele-Shaw cell was really two dimensional. However, the cell lives in a three-dimensional world in which there are two radii of curvature for the surface. The larger one, $R$, has the smaller effect upon the pressure drop, while the smaller one (which is roughly $b/2$) dominates. Hence Eq. (1.5a) makes very little experimental sense. Park and Homsy (1984) suggested an alternative boundary condition that might better describe a situation in which a fluid that wets the plates is displaced by one that does not. From an asymptotic analysis they derived an expression for the pressure jump that one should use instead of Eq. (1.5a),

$$\Delta P = \frac{T}{b/2}\left[1+3.80\left[\frac{\mu v_n}{T}\right]^{2/3}\right]+\frac{\pi}{4}T\kappa \ . \tag{1.5b}$$

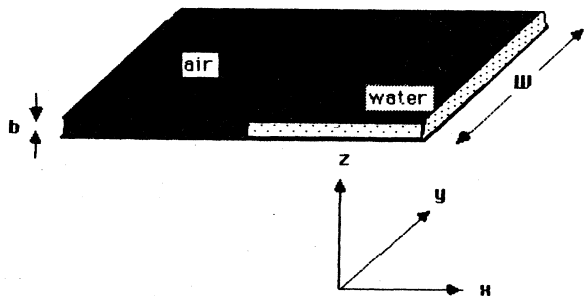


FIG. 1. Hele-Shaw cell and our coordinate system.

The first term in Eq. (1.5b), $2T/b$, is independent of $x$ and $y$, so it does not really affect the motion. The other two terms act together, producing forces that tend to flatten out the interface.

We shall look at the simplest possible situation. Let the plates be very long rectangles with width $W$ (Fig. 1). The second fluid is, say, air, so that we may take it to have a negligible density and viscosity. Let the first fluid be, say, water and let the air be pushing it so that it moves with an average velocity $U$. The plates are horizontal, so that gravity does not enter.

The side walls are rigid. This is represented by using a slip boundary condition, so that at the side walls the normal component of the velocity vanishes:

$$(\boldsymbol{v})_n = 0 \ . \tag{1.6}$$

This free slip boundary condition may not be realistic for the true experimental situation, but it may be an essentially correct approximation for small $b$, where there is a boundary layer of width $b$ near the surface over which $\boldsymbol{v}$ may vary quite rapidly.

Now, in both experiments and simulations, one observes three different types of motion.

Case A. Small $U$ or negative $U$. (The latter implies that the water is pushing on the air.) An initial interface, which perhaps has a few bumps in it, eventually flattens out and forms a straight boundary between the two fluids.

Case B. Intermediate $U$. Any initially present bump grows and forms a stable finger (Fig. 2). The width of the finger is a multiple, $\lambda$, of the channel width $W$ and varies with velocity. Under the stated conditions, in which we can neglect the second fluid, there is only one dimensionless parameter[1] entering these equations, namely,

$$d_0 = \frac{\pi^2}{3}\frac{b^2}{W^2}\frac{T}{\mu U} \ , \tag{1.7}$$

which, therefore, acts as a control parameter. Here $U$ is the fluid velocity in the region far downstream from the finger. We call $d_0$ the "surface-tension parameter." The dependence of the finger width on $d_0$ is an interesting quantity to predict theoretically. Below, we discuss our results for this dependence and those of others.

Case C. Large $U$. Hence the surface-tension parameter $d_0$ is very small. In this domain, several types of time-dependent behavior may be observed. For the very largest values of $U$ a kind of chaotic behavior is observed in which several fingers are formed that may branch and split (Fig. 3). There is a tendency for the tallest fingers to get ahead and leave the smaller ones well behind. Thus there is essentially a cascade into large length scales, which saturates when the fingers become of width comparable to that of the cell. Even if there is only one finger in the channel, for these large values of $U$ the finger tends to wiggle up and down, partially split, and in general to show quite an unstable behavior.

As we shall see below, the theory suggests that, even for the largest values of $U$, if one waits long enough, the system will settle down into a single stable finger. The splitting observed in simulations and experiment is, according to the theory, an "artifact" produced by the noise in the system. However, for very small values of the surface tension this artifact is almost unavoidable since the noise required to split the finger is very small indeed. Below, we shall present evidence that the critical size of a perturbation required to destabilize the finger is a distortion of a size that is exponentially small, specifically $\exp(-\text{const}/\sqrt{d_0})$. Hence, for very small values of the surface-tension parameter $d_0$, the observed behavior is always quite noisy.

### B. Stability analysis (Chuoke *et al.*, 1959)

The first step is to look at the stability of an almost-flat interface. Let the flat interface be at a position $x(y)=Ut$, which moves with velocity $U$ relative to the walls. A small deviation from flatness may be represented by writing

$$x(y) = Ut + A(t)\cos qy \ , \tag{1.8a}$$

where $A(t)$ is considered to be small. If $A$ vanished, the velocity $U$ would be produced by a pressure gradient $-U/(b^2/12\mu)$. If we add to this zero-order term a term produced by the deviation from flatness, we find a result like Eq. (1.8a), namely,

$$P(x,y) = P_0 - \frac{U}{(b^2/12\mu)}(x-Ut) + B(x,t)\cos qy \ .$$

For $P(x,y)$ to obey Laplace's equation $B(x,t)$ must vary as $e^{qx}$ or $e^{-qx}$. The former is impossible if the pressure is to remain finite as $x \to \infty$. Thus we find

$$P(x,y) = P_0 - \frac{U}{b^2/12\mu}(x-Ut) + B(t)e^{-qx}\cos qy \ , \tag{1.8b}$$

where $P_0$ is constant. The boundary condition at the side walls then requires the wave vector $q$ to be

$$q = \frac{2\pi n}{W} \ , \tag{1.9}$$

where $n$ is a positive integer.

If $A$ is small, Eq. (1.8a) gives the velocity of the interface as

$$U_n = U + A(t)\cos qy \ .$$

On the other hand, the Darcy equation (1.1) and pressure equation (1.8b) together imply

[1]Since there is no agreement on the exact form of the surface-tension parameter, we shall, for the convenience of the reader, relate our parameter $d_0$ to the one used by other workers in the field. Thus the parameter $\kappa$ used by McLean and Saffman (1981) is $\kappa = d_0\lambda/(1-\lambda)^2$. The parameters $B,\tau$ introduced, respectively, by Tryggvason and Aref (1983) and DeGregoria and Schwartz (1986) are $\tau = B = d_0/(2\pi)^2$.

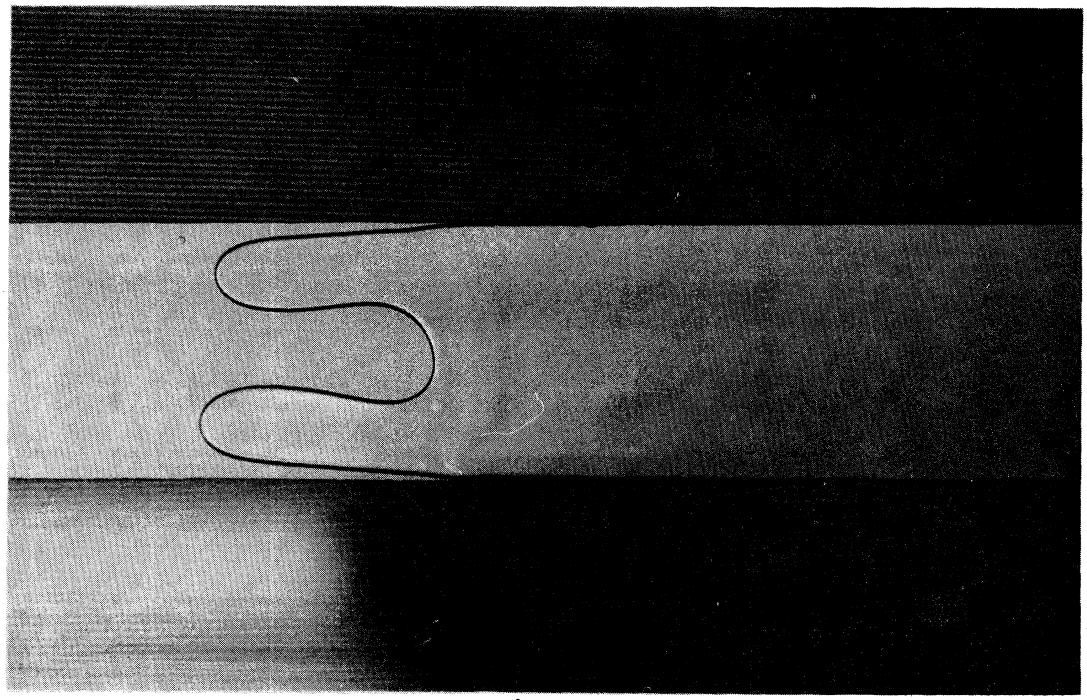

(a)

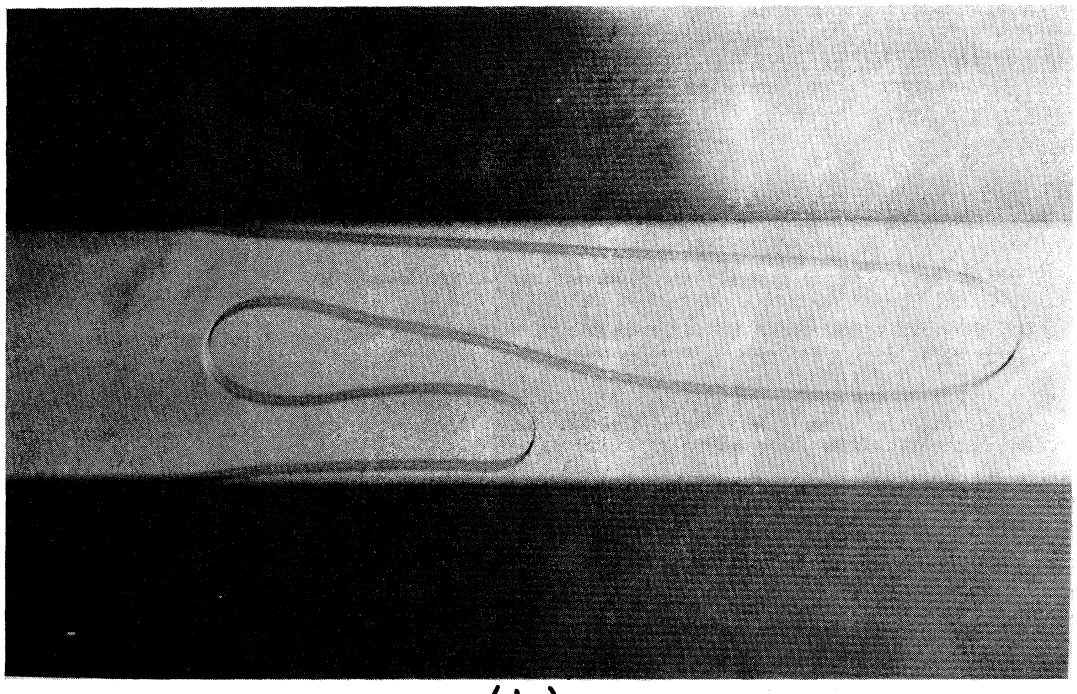

(b)

FIG. 2. Competition between two bumps leading to the emergence of a single propagating finger, courtesy of Tabeling and Libchaber (1986). Parts (a), (b), and (c) represent successively later times in the development of the same run.

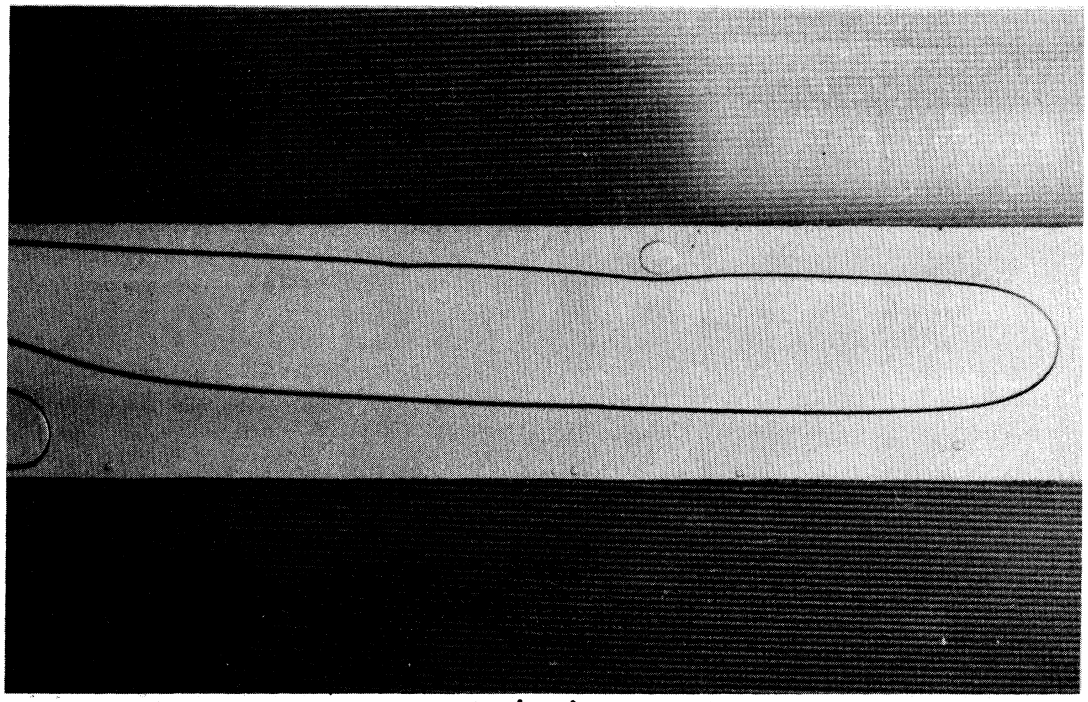


FIG. 2. (*Continued*).

$$U_n = U + \frac{b^2}{12\mu} qB(t)\cos qy$$

if we neglect terms of order $A^2$ or $AB$. In this way we derive two equations for $U_n$ and thus get one relationship between $A$ and $B$, namely,

$$\dot{A}(t) = B(t)\frac{b^2}{12\mu} q \ . \tag{1.10}$$

The final relationship is derived by calculating the terms in the pressure jump that are proportional to $\cos qy$, using the fact that pressure in the air is constant. On the one hand, from Eqs. (1.8a) and (1.8b), this part of the pressure jump is

$$\Delta P(y) = \left[ \frac{U}{b^2/12\mu} A - B \right] \cos qy \ . \tag{1.11}$$

On the other hand, Eq. (1.5a) gives the pressure jump as

$$\Delta P(y) = -T\kappa \approx -T\frac{d^2}{dy^2} x(y) \ . \tag{1.12}$$

Setting this result together with Eqs. (1.10) and (1.11) one finds that $A$ satisfies

$$\dot{A} = A\left[ \frac{U}{b^2/12\mu} - Tq^2 \right] \frac{b^2}{12\mu} q \ . \tag{1.13}$$

This result is easily interpreted. First of all, notice that when the quantity in parentheses is positive the flat interface is unstable; when it is negative the interface is stable against a disturbance of the given wave number. Since, according to Eq. (1.9), the minimum value of $q$ is $2\pi/W$, the flat interface will be unstable against some perturba-

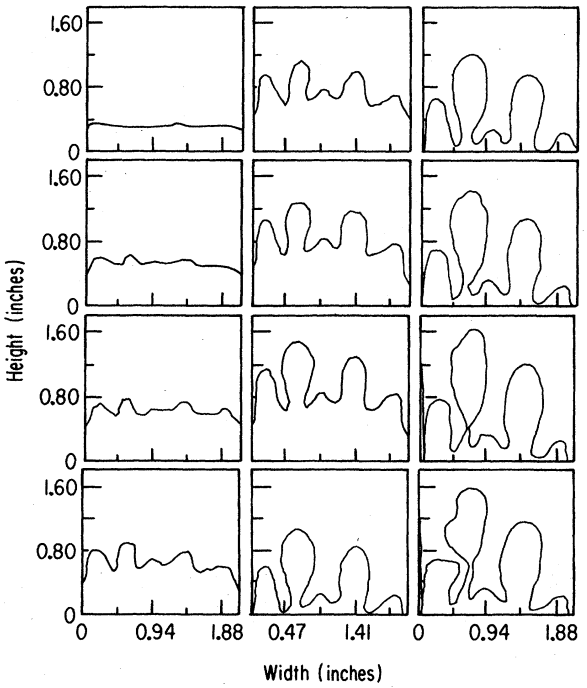


FIG. 3. Chaotic behavior in a Hele-Shaw cell filled with fluids of similar viscosities, courtesy of Maher (1985). Time goes from top to bottom and then from left to right.

tion whenever the surface-tension parameter defined by Eq. (1.7) obeys $d_0 < 1$.

Alternatively expressed, a very long interface will be unstable against a perturbation of wavelength $l = 2\pi/q$ whenever $l > W\sqrt{d_0}$. Hence for very small surface tension, the system will be unstable against even very short wavelength perturbations.

The physical source of this instability lies in the geometry of the moving interface. Imagine a situation in which the pressure difference along the length of the channel is fixed. Then, since the pressure in the air is constant, the larger gradients in the pressure appear at the end of the largest fingers of air. Hence these fingers move faster than the rest. Hence they get further ahead. The entire system is, in this way, destabilized by the motion.

Conversely, the surface tension tends to stabilize and smooth out the smallest fingers, those with a radius of curvature less than $W\sqrt{d_0}$. These smallest fingers have at their ends a large pressure drop from across the air-water interface. Water flows in toward these low-pressure regions, pushing the smallest fingers backward. Hence they are smoothed out by the surface tension.

If we use instead of the two-dimensional jump condition, Eq. (1.5a), the three-dimensional condition, Eq. (1.5b), the resulting equation for the amplitude is

$$\dot{A} = \frac{Uq - \frac{\pi}{4} T q^3 b^2/12\mu}{1 + 0.42 qb (T/\mu U)^{1/3}} A \ . \tag{1.14}$$

Equations (1.13) and (1.14) have qualitatively similar properties. In both cases something very peculiar happens when the surface tension goes to zero. Then the most unstable wavelength becomes shorter and shorter. In the limit $T \to 0$, the shortest wavelengths are the most unstable. One suspects that, in this limiting case, the entire physical problem may well be poorly defined.

### C. The small-surface-tension puzzle

Let us for a moment ignore the problem of the short-wavelength instability in the absence of surface tension and ask about the steady states only. In their classic paper, Saffman and Taylor (1958) found a one-parameter family of finger-shaped steady-state solutions. These solutions correspond to different values of $\lambda$, the ratio of the finger width to the width of the cell. The finger shape is described by the formula to be given in Sec. III,

$$\frac{x}{W} = \frac{(1-\lambda)}{\pi} \ln \cos \left[ \frac{\pi y}{\lambda W} \right] . \tag{1.15}$$

These shapes seemed to be quite similar to those that were observed experimentally. However, there were two serious problems. First, in the experiment, a finger of a well-defined width was observed at each given velocity. The zero-surface-tension theory could not predict that, since by varying $\lambda$ one could obtain fingers of any width at all. Second, from our analysis above, one should expect the $T = 0$ solutions to be completely unstable, while the fingers that were observed were quite stable. Both problems are related to the singular nature of the zero-surface-tension limit. Another point made by Saffman and Taylor in their paper was the fact that no fingers with $\lambda$ less than $\frac{1}{2}$ were seen in the experiment at all, and they asserted that $\frac{1}{2}$ was the asymptotic width of the finger in the $d_0 \to 0$ limit.

The question of "velocity," or finger width $\lambda$, selection was again taken up by McLean and Saffman (1981), who looked for the steady-state solutions in the presence of a small but finite surface tension. Numerically solving the integral equation for the interface, they found a unique solution for a given value of $d_0$, rather than a one-parameter family. Their work was further extended by Vanden-Broeck (1983), who found not just one, but a discrete set of solutions. However, for all of his solutions, as $d_0$ goes to zero, $\lambda$ goes to one-half.

Thus the "degeneracy" of the steady states is lifted by the effects of the surface tension, which is a *singular* perturbation in this problem [see Bender and Orszag (1978) for a discussion of singular perturbations]. This phenomenon, common to a large class of nonlinear problems arising in physics, was studied by Barenblatt and Zel'dovich (1972; see also Barenblatt, 1979) in the general context of similarity solutions to partial differential equations. (The propagating solution, such as the Saffman-Taylor finger, may be thought of as a kind of similarity solution as well.) Barenblatt and Zel'dovich point out that in cases where singular perturbations are involved, the search for the similarity solutions leads to nonlinear eigenvalue problems. These eigenvalues then determine the scaling, or in case of propagation, the velocity, of the similarity solution. The existence of a continuous family of solutions would then correspond to a continuous spectrum. More commonly a discrete spectrum is found. Thus the work of McLean and Saffman and Vanden-Broeck fit nicely into this general[2] framework.

---

[2]There is reason to believe that some of the other puzzling "selection" problems will be resolved along the same lines. For example, recently Pelcé and Pomeau (1986a, 1986b) derived a nonlinear eigenvalue equation governing the shape and velocity of a dendrite (in the low-Peclet-number limit of the "two-sided" model). The work of Barenblatt and Zel'dovich (1972) also largely anticipated the "microscopic solvability" principle put forward by Kessler, Koplik, and Levine (1984, 1985a) and Ben-Jacob and co-workers (1984) to explain the growth velocities in their models of solidification. See also recent work of Meiron (1986) and Kessler and Levine (1986a). As this paper was completed, work by Shraiman, by Hong and Langer, and by Pomeau and co-workers was reported to us in preprint form. P. Saffman reported to us verbally on his work. All these authors have studied time-independent solutions to the Saffman-Taylor problem in the small-surface-tension limit. They conclude that the singular perturbation produces a stable finger and that for small $d_0$, $\lambda - \frac{1}{2}$ has a discrete spectrum. The lowest value of the width has $\lambda - \frac{1}{2}$ proportional to $d_0^{2/3}$.

The results of McLean and Saffman (1981) and Vanden-Broeck (1983) produced a theoretical prediction for the finger-width dependence on the control parameter. Alas, the stability problem remained unresolved since the analysis performed by McLean and Saffman found that the fingers remained unstable even in the presence of surface tension. This was a result contradictory to the experiment and numerical simulations. Hence the point about stability remained open.

All of these difficulties arise from the subtlety of the zero-surface-tension limit, which is singular indeed. In fact, the short-wavelength instability leads to the appearance of finite-time singularities in the dynamical equations for a large class of initial conditions, as was shown by Shraiman and Bensimon (1984) and Sarkar (1984); see also the work of Meyer (1982) and Howison (1985). These singularities correspond to $\frac{2}{3}$ power cusps in the interface. After the appearance of the cusp the calculations (and probably the solutions) break down. Some of the time-dependent solutions evolving into such cusps can be found explicitly (Meyer, 1982; Shraiman and Bensimon, 1984; Howison, 1985). While many initial conditions lead to cusps, there are also some special initial conditions that give instead $\lambda=\frac{1}{2}$ steady fingers. These $T=0$ results can be derived using the conformal mapping method, which we shall describe in Sec. III.

In the last year, as a result of the experimental studies of Tabeling and Libchaber (1986) and the theoretical work of Kessler and Levine (1986a, 1986b), DeGregoria and Schwartz (1986), and Bensimon (1986), a new understanding of the stability problem began to emerge. [See also the earlier experiments of Aribert (1970), as well as the more recent work of Maher (1985).] First of all, experimentally the fingers at high velocity (small $d_0$) *are* unstable (a fact that was observed, but for some reason ignored in Saffman and Taylor, 1958). Naively, one can try to explain this by noting that, for small values of the surface-tension parameter $d_0$, the unstable wavelength $l=W\sqrt{d_0}$ is much shorter than the characteristic curvature and width of the finger. Thus on the length scale $l$ the finger appears to be essentially flat and therefore should be unstable. If this were indeed the case one would expect the finger to become unstable at $d_0\approx 1$, that is, shortly after the "primary" instability, which led to the appearance of the finger in the first place. Instead, the instability is observed at $d_0\sim 10^{-2}$ and a different scenario is required. Kessler and Levine (1985b) suggested that the interaction of the finger with the rigid walls makes the finger stable with respect to infinitesimal perturbations [contrary to the result of McLean and Saffman (1981)]. This was corroborated by the observation by DeGregoria and Schwartz (1986) that in the numerical simulations the disturbances generated at the tip decay in amplitude as they are subvected along the side of the finger. DeGregoria and Schwartz (1986) and Bensimon (1986) then proposed that the experimentally observed behavior is due to a finite-amplitude instability. Furthermore, from numerical stability analysis and simulations Bensimon found that the noise amplitude required for destabilization decreases rapidly with $d_0$ and is consistent with the expression

$$\ln(\text{noise})\sim -d_0^{-1/2} \tag{1.16}$$

(see Sec. V.D below). He also found the most unstable modes, which are in excellent agreement with the experiments of Tabeling and Libchaber (1986).

The physical mechanism involved here appears to be very similar to the one proposed earlier by Zel'dovich and co-workers (1980) in connection with the stability of cellular flames. The growth rate of a disturbance is proportional to the normal velocity of the interface, so that it is large at the tip and approaches zero toward the side of the fingers. As the finger moves forward, the disturbance moves more slowly than the tip, so that it gradually moves toward less unstable regions. When the instability becomes weak, even a little surface tension is sufficient to damp out the disturbance. In Sec. V we shall derive the result (1.16), using these ideas of Zel'dovich and coworkers (1980).

Another result that emerged from various theories and simulations is the dependence of the finger width $\lambda$ on the surface-tension parameter $d_0$ (shown in Fig. 7 below). While the dependence is similar to that observed in the experiment, the direct comparison is not satisfactory. The reason is that the theorists have simplified the problem by assuming that the pressure jump on the interface is velocity independent [Eq. (1.5a)], rather than a more appropriate condition given by Eq. (1.5b). Zocchi, Tabeling, and Libchaber (1986), in very careful experiments, have demonstrated the importance of the wetting film left behind a Saffman-Taylor finger on the determination of the finger width and on its destabilization. They have shown that the predictions based on the Saffman-Taylor model, Eq. (1.5a), i.e., on a single control parameter $d_0$, were not compatible with the outcome of the experiments, which seemed to depend on two control parameters: the surface-tension parameter $d_0$ and the aspect ratio $W/b$ (see Fig. 4). For nonwetting fluids, however, the Saffman-Taylor model may be an adequate description of the experimental situation, although because of the difficulty of working with nonwetting fluids this has not yet been checked.

## II. RANDOM-WALK MODELS OF HELE-SHAW BEHAVIOR

The Saffman-Taylor problem involves solving the Laplace equation for the pressure with appropriate boundary conditions. If one has a random walker moving through any volume of space, the probability that the walker will land on a given site $P(\mathbf{r})$ also obeys Laplace's equation. This mathematical analogy can be used to set up a conceptual model equivalent to the Hele-Shaw system in which, instead of fluid flow, one has the motion of random walkers. It is closely related to another much-studied model, diffusion-limited aggregation, and it pro-

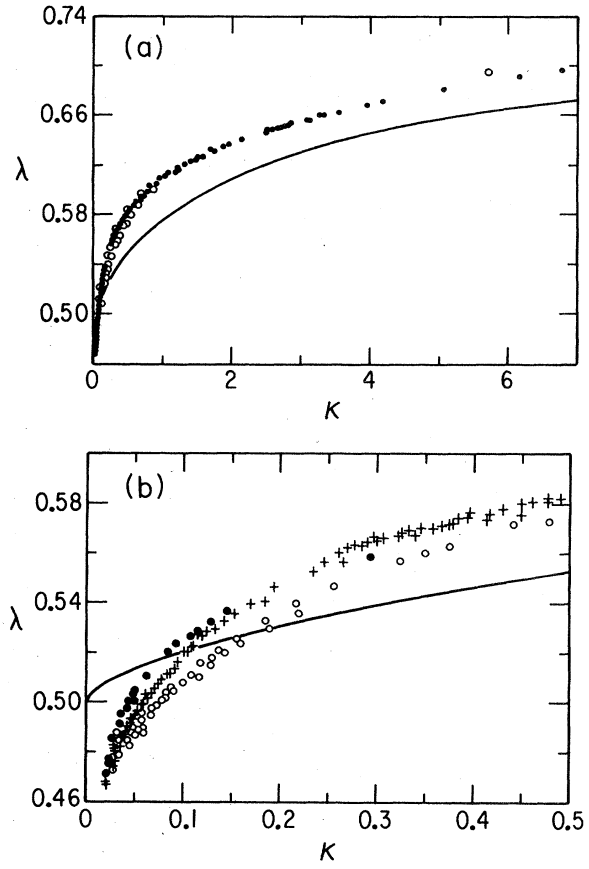


FIG. 4. Finger width $\lambda$ as a function of the control parameter $\kappa\{\kappa=[\lambda/(1-\lambda)^2]d_0\}$ for various aspect ratios $W/b$. Experimental data courtesy of Zocchi, Tabeling, and Libchaber (1986). Solid curve, McLean-Saffman numerical result. (a) $0\leq\kappa\leq 7$. ●, $W/b=65$; ○, $W/b=27.5$. (b) $0\leq\kappa\leq 0.5$. ●, $W/b=112.5$; +, $W/b=65$; ○, $W/b=27.5$.

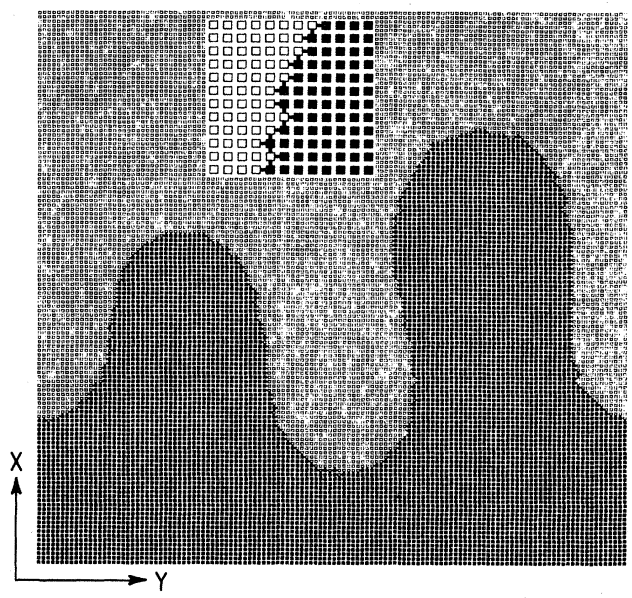


FIG. 5. Setup for random-walk simulation. The black region represents air in the Hele-Shaw cell, and the white region, water. Random walks take place in the white region. Between every pair of adjacent sites of different colors, there is a bond (see the inset) that contains a number. The air-water interface moves according to these numbers. While all random walks terminate at the interface, they may start either from a horizontal line above the interface, which provides an upward pressure gradient, or from the interface itself, which rearranges the interface and represents the surface tension.

vides a useful visualization of the Hele-Shaw system. The DLA analogy may be used to gain insights about the hydrodynamic system. Finally, the random-walk picture may be translated into a quite effective computer model of the Hele-Shaw flow and provides the foundation for a Monte-Carlo simulation of the hydrodynamic process.

The DLA model was invented by Witten and Sander (1981, 1983) to describe aggregation of small particles. In the variant of the model of particular interest here, there is a square lattice on which each site is occupied by air (shown as the black region in Fig. 5) or water (shown as the white region in Fig. 5). In the DLA picture, the aggregate is the air region; the empty space corresponds to the high-viscosity fluid. Random walkers are released far from the aggregate. They move about until they wander over an air-water bond. As they cross the bond, the air advances by one unit occupying the last site visited by the walker. Then the process begins again.

The differential equations are simple. The probability that a site will be visited obeys the lattice version of $\nabla^2 P=0$. If the walkers are reflected at the side walls, then on them $(\nabla P)_n=0$. Since the probability vanishes inside the air region, we have on the air-water interface $P(r)=0$. Finally, the average "speed" at which a piece of interface advances is proportional to the probability just on the "water" side of the interface, which is then proportional to the normal component of $\nabla P$, i.e.,

$$v_n=(\nabla P)_n \ . \tag{2.1}$$

Thus DLA looks like the zero-surface-tension version of the Saffman-Taylor problem. This analogy was also noticed by Pietronero and Wiesmann (1984) in the context of dielectric breakdown.

Now comes an interesting fact. Recall that zero-surface tension produces a highly unstable interface. In DLA the interface is so unstable as to produce a fractal structure in which the aggregate forms tiny fingers or wisps that split and split and split again. This does not look like any structure produced in a real fluid flow for which $T\neq 0$. (Perhaps it does represent what we would see if we were to take $T$ to zero.)

Our group at the University of Chicago, and in parallel Szép, Cserti, and Kertész (1985) in Hungary, carried out rather similar investigations of how DLA might be

changed to better reflect fluid flow. There are two major problems.

(1) Because the walkers arrive one at a time, the surface motion is jumpy and grainy. Some kind of averaging is needed to smooth out the noise.

(2) The lack of surface tension produces an unstable interface whenever the air moves into the water.

Chao Tang (1985) showed how to solve problem (1) and evade problem (2) thereby generating a situation in which one could confirm the relationship between DLA and the Saffman-Taylor problem. He smoothed out the behavior by requiring that no motion occur until some number $M$ of walkers arrived. When $M$ was large, say, 20 to 100, he could get a far less noisy situation. To eliminate the instability, problem (2), he investigated situations in which the air was moving backward, away from the water. (See also Paterson, 1984.) This change was achieved by allowing the water to advance by one unit whenever $M$ walkers arrived. When he then compared his result to the exact steady-state solution of Saffman and Taylor (1958) or to the exact time-dependent solution of Shraiman and Bensimon (1984), he found an excellent agreement between his numerical, random-walk-based simulation and the exact solution.

In parallel the Hungarian group, Szép *et al.* (1985), and Kadanoff (1985) suggested a method of improving the DLA model to include surface tension correctly. The problem is to get $P(r)$ at the interface to have a value of the form

$$P(r)=A\kappa+B\ , \tag{2.2}$$

where $A$ will be proportional to the surface tension. The solution is to allow walkers to leave the air-water interface, walk through the water, and finally stop when they reenter the water. If one allows the walkers to leave with a probability of the form of Eq. (2.2), measures the net flux of walkers through each interface bond, and then moves the air or water forward whenever that flux is $-M$ or $M$, one has the model that was very successfully applied by Liang (1986) and also essentially the model developed independently by the Hungarian group. The curvature is estimated by a method due to Vicsek (1984).

This kind of simulation gives, as it should, a stable flat interface when $d_0 > 1$. If one starts from a geometry that looks like a finger, a stable finger develops in the simulation for $d_0$ greater than about 0.05 (see Fig. 6). The $\lambda$ vs $d_0$ plots agree well with previous numerical calculations (Fig. 7) [McLean (1981), Tryggvason and Aref (1983)], and the finger shape agrees reasonably well with the experimental observations of Pitts (1980; see Fig. 8). According to the fundamental theory, the fingers should remain stable even as $d_0 \to 0$ in a noise-free environment. However, the theory also predicts that the fingers would be extremely sensitive to noise for small values of $d_0$. Hence it is not surprising that the simulations, which certainly must contain a bit of noise, show an instability for small $d_0$. In the simulations, as $d_0$ gets smaller, the finger first becomes slightly asymmetric [Fig. 9(a)], then for smaller $d_0$ the tip of the finger splits [Fig. 9(b)], and for the smallest values of $d_0$ [Fig. 9(c)] a highly branched and apparently dendritic structure is produced.

Experiments see the asymmetry and the splitting, but

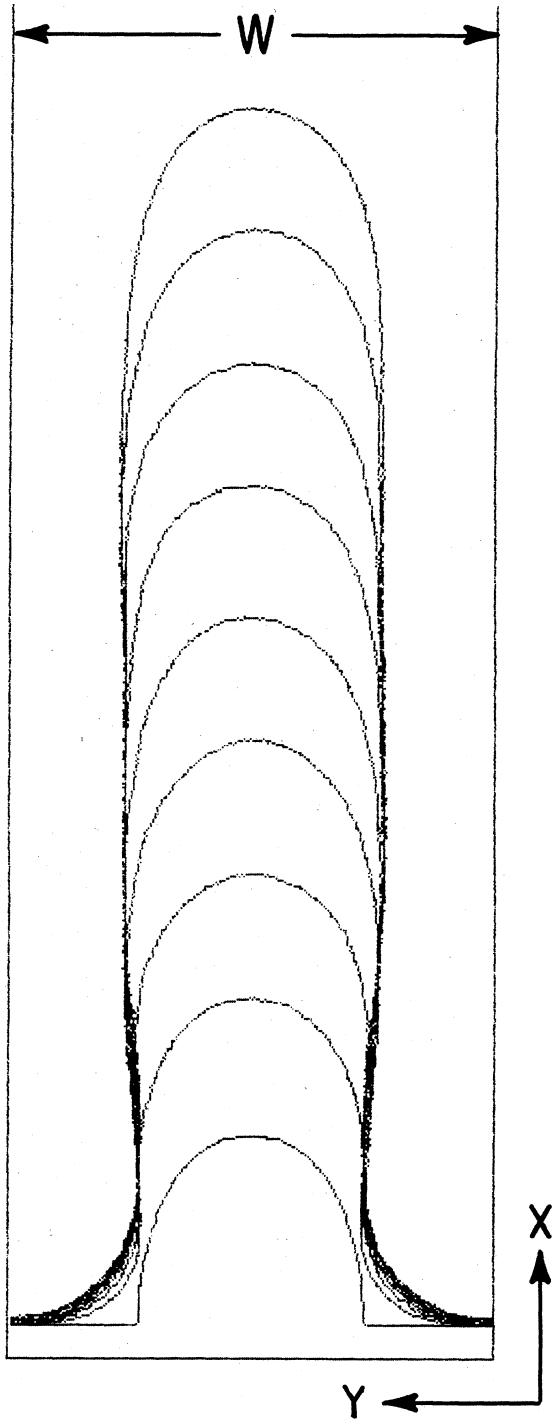


FIG. 6. Evolution of a stable finger. The successively higher curves represent later stages in the finger development. From Liang (1986).

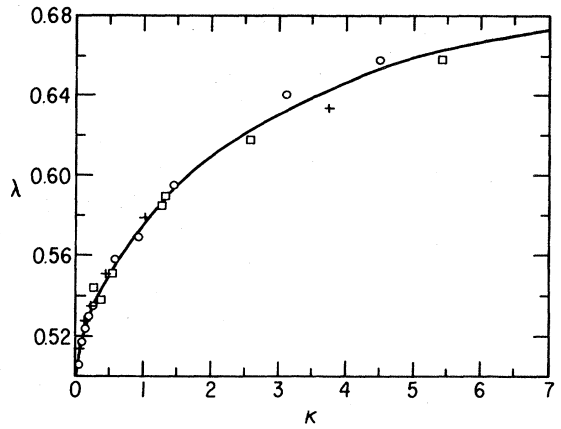


FIG. 7. Finger width $\lambda$ as a function of the control parameter $\kappa$ $\{\kappa=[\lambda/(1-\lambda)^2]d_0\}$: solid curve, McLean-Saffman (1981) numerical result; ○, simulations of Bensimon (1986); +, simulations of DeGregoria and Schwartz (1986); □, random-walk simulations of Liang (1986).

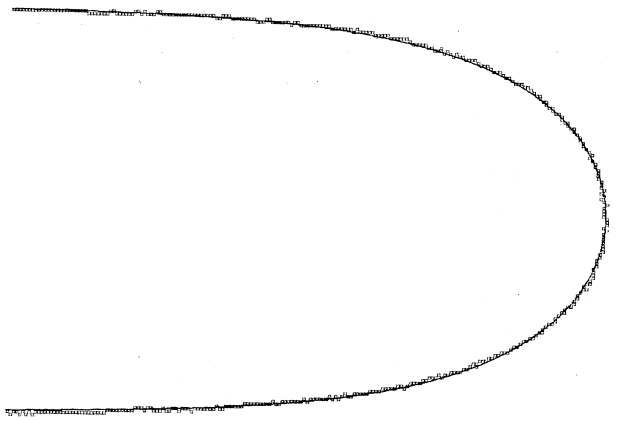

FIG. 8. Comparison of the finger shape obtained from simulations and experiment. □, random-walk simulation (Liang, 1986); solid curve, Pitt's (1980) phenomenological scaling hypothesis, which agrees with the experimental data of Saffman and Taylor (1958).

as far as we know no Hele-Shaw experiment in a Newtonian fluid[3] has ever shown an apparently fractal structure like that in Fig. 9(c).

Since the experiments contain noise, it is not surprising that they show a structure analogous to the simulations of Figs. 9(a) and 9(b). However, the dendritic structure of DLA and of the simulations might be a pure artifact of the details of the model and might not really be expected to appear in any fluid system. In the end, we must say that we still do not fully understand what happens in the Saffman-Taylor problem for very small values of the surface tension. Neither experiment nor the random-walk simulations can settle this, since they are both too sensitive to noise and small perturbations. Some evidence can be obtained from more fundamental theory, which is the subject of the next section.

## III. THE HODOGRAPH METHOD

### A. Complex analytical methods

In this section we summarize what is known about the Saffman-Taylor problem at zero-surface tension. We shall describe a method, involving analytic functions of complex variables, which enables one to study the dynamics of the interface evolution in the absence of surface tension.

[3]Nittman, Daccord, and Stanley (1985) have indeed seen a structure roughly like this. However, their comparison with DLA is somewhat misleading because they have used the wrong equations for a non-Newtonian fluid and the wrong boundary conditions for a Newtonian one.

In Sec. I the Saffman-Taylor problem was formulated mathematically in terms of a Laplace equation for the pressure (or velocity potential) with two boundary conditions. As is usual in two-dimensional problems involving the Laplace equation, one can be helped considerably by using complex variable techniques (Carrier, Krook, and Pearson, 1966). The basic idea is to think of the velocity potential $\varphi(x,y)$ as the real part of a complex field,

$$\Phi(x,y)=\varphi(x,y)+i\psi(x,y) . \tag{3.1}$$

The requirement that $\nabla^2\varphi=0$ can be automatically satisfied simply by requiring that $\Phi$ be an analytic function of the complex variable

$$z=x+iy . \tag{3.2}$$

For reasons that will become more obvious later, it is better to invert the functional dependence and, instead of describing how $\Phi$ is determined by $z$, rather say that the potential $\Phi$ defines where we are in space. In symbols,

$$z=f_t(\Phi) . \tag{3.3}$$

The subscript $t$ indicates that the dependence changes in time. In fact, we shall use the boundary conditions, Eqs. (1.4) and (1.5) to define the time dependence of $f$.

Equation (3.3) is the central equation in the hodographic method, widely used in fluid mechanics. For the Saffman-Taylor problem, the hodograph technique has been used to obtain a partial solution in the absence of surface tension (see Secs. III.C and III.D below), to do simulations (as discussed in Sec. IV below), and to discuss the stability of small-surface-tension solutions (see Sec. V below).

### B. Basic equations

The real velocity potential $\varphi(x,y)$ is defined so that its gradient is the velocity vector. The corresponding state-

ment for the complex case is that

$$v_x(x,y)-iv_y(x,y)=\frac{d}{dz}\Phi(z)\ . \tag{3.4}$$

Equation (3.4) can then be reexpressed to give several useful boundary conditions. Since $v_y$ vanishes on the side walls, $y=\pm W/2$, the imaginary part of $\Phi$ must be constant on each wall. We denote the velocity downstream

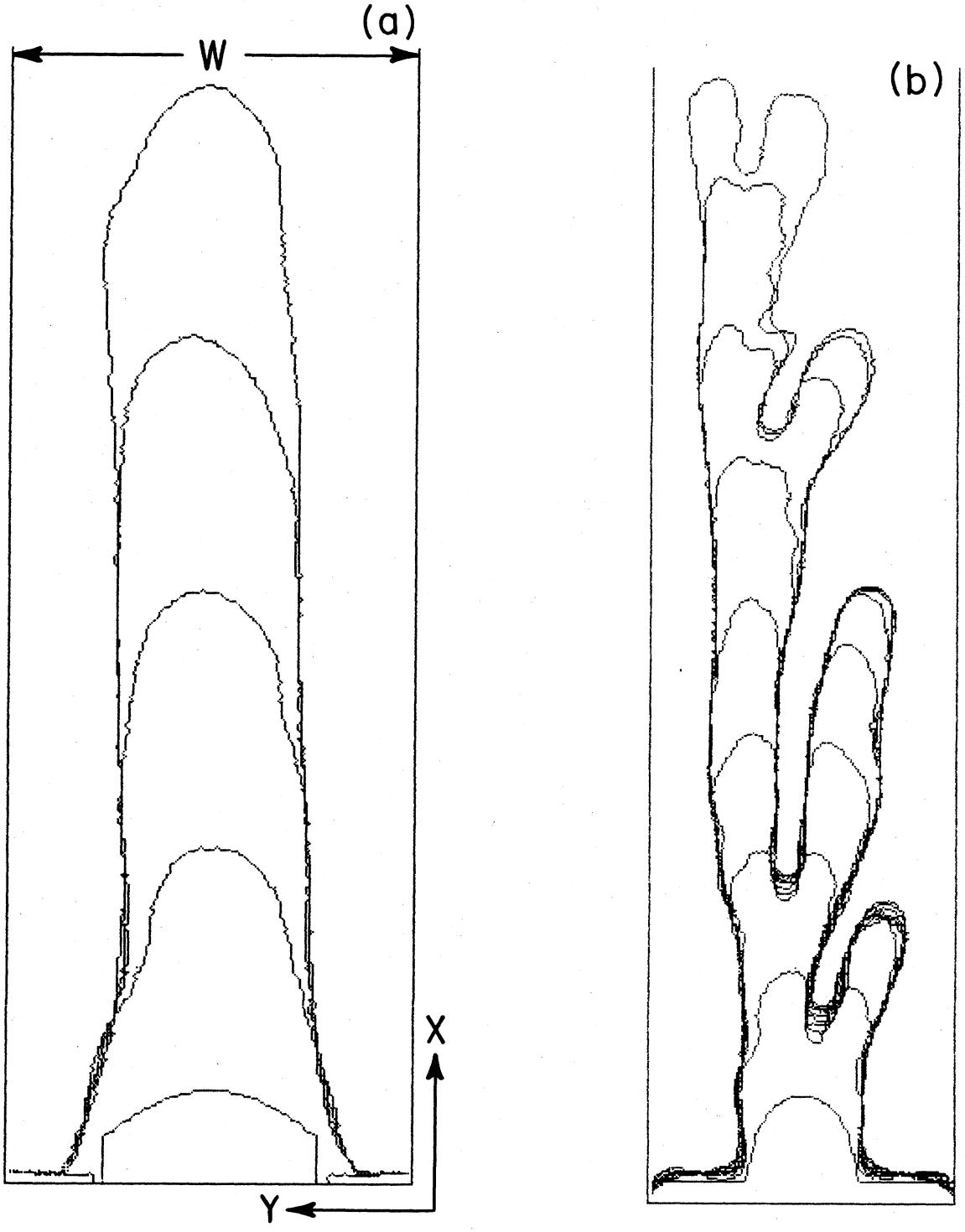


FIG. 9. Some of the unstable modes observed in random-walk simulations, from Liang (1986). Motion is toward the top. (a) At the onset of instability, the finger becomes asymmetric. (b) At smaller surface tension, beginning of tip splitting. (c) At even smaller surface tensions the finger evolves into a very ramified structure.

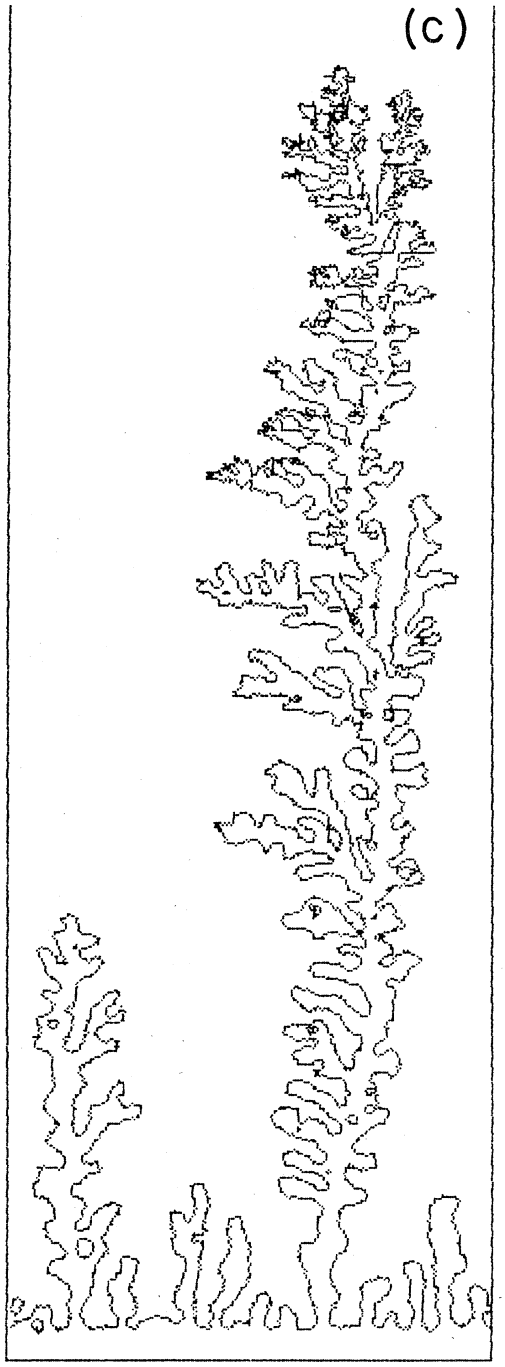


FIG. 9. (*Continued*).

by $U$. Then, since $v_y$ vanishes far downstream, we see that $\Phi \to Uz + \text{const}$ as $\text{Re}(z) \to \infty$. When we take the constant to be real, we see that $\text{Im}\Phi = \pm UW/2$ on the two walls.

What we have just said can be converted into boundary conditions upon the unknown function $f_t$ of Eq. (3.3), i.e.,

$$\text{if } \text{Re}\Phi \to \infty, \text{ then } f_t(\Phi) \to \frac{\Phi}{U} + C_0 \text{ with } \text{Im}C_0 = 0 ; \tag{3.5a}$$

$$\text{if } \text{Im}\Phi = \pm UW/2, \text{ then } \text{Im}f_t(\Phi) = \pm W/2 . \tag{3.5b}$$

Finally, at zero-surface tension, the pressure, and hence the velocity potential, is constant on the interface between the two fluids. Thus, if we take this constant to be zero, we can choose $\Phi$ to be of the form $is$ for $s$ real, on the interface.

To define the interface more precisely we must determine a curve for each value of the time $t$. One way of doing this is to define a complex function of two real variables, $s$ and $t$, i.e., $\gamma(s,t)$. For each value of $t$, as $s$ sweeps over its entire range, $\gamma(s,t)$ sweeps over a set of points $z_t(s)$. These points are the complex variables that give the values of $x+iy$ for all $x$ and $y$ on the interface. This function $\gamma(s,t)$ is thus the solution to our problem. The third boundary condition is that, in the case of zero-surface tension,

$$\gamma(s,t) = f_t(is), \quad s \in \left[ \frac{-UW}{2}, \frac{UW}{2} \right] . \tag{3.5c}$$

Notice that the three boundary conditions, Eqs. (3.5), have defined the physical region of $\Phi$ to be the strip

$$\Phi = \varphi + i\psi, \quad -\frac{UW}{2} \le \psi \le \frac{UW}{2}, \quad 0 \le \varphi \le \infty . \tag{3.6}$$

Within this strip, $f_t$ must be analytic and its derivative must be nonzero. These two conditions together ensure that $\nabla^2 \varphi = 0$ in the region filled by water.

One more condition must be fulfilled: the interface must move with the same velocity as the fluid. Consider the time dependence of $\gamma(s,t)$. For each value of $s$, $\gamma(s,t)$ specifies the value of $x+iy$ for some point on the interface at time $t$. An infinitesimal time interval later, this same piece of fluid will have moved forward by an amount $(v_x + iv_y)dt$. In this way, we find one term in the time derivative of $\gamma$;

$$\frac{d}{dt}\gamma(s,t) = v_x + iv_y . \tag{3.7a}$$

Using Eq. (3.4), we can rewrite Eq. (3.7a) as

$$\frac{d}{dt}\gamma(s,t) = \left[ \frac{d\Phi}{dz} \right]^* = \frac{1}{(dz/d\Phi)^*} = \frac{-i}{\partial_s \gamma(s,t)^*} . \tag{3.7b}$$

The total derivative on the left-hand side of Eq. (3.7b) represents the possibility that, as the front advances, the value of the parameter $s$ labeling a particular piece of fluid might change. If it does this at a rate $ds/dt$, then we must add to Eq. (3.7b) a term reflecting this change to obtain

$$\partial_t \gamma(s,t) = -i \frac{\partial_s \gamma(s,t)}{|\partial_s \gamma(s,t)|^2} - \frac{ds}{dt}(s,t)\partial_s \gamma(s,t) . \tag{3.8}$$

Equation (3.8) will determine the motion of the interface. At first sight, it does not look as if the derivation of Eq. (3.8) represents much progress. For one unknown function, $\gamma(s,t)$, we have traded another, $ds/dt$. In fact, however, a considerable advance has been made. We know that $\gamma(s,t)$ is analytic and has a nonzero derivative for all values of $s$ in the strip [Eq. (3.5c)]. This analyticity essentially determines the parametrization of $\gamma(s,t)$. In turn, the analyticity, plus the condition that $ds/dt$ is real, fully determines the solution to Eq. (3.8).

There are several different methods for obtaining solutions to Eq. (3.8). The easiest is to eliminate $ds/dt$ by multiplying by the complex conjugate of $\partial_s\gamma$ and then taking the imaginary part of the result, to find

$$\partial_t\gamma(s,t)\partial_s\gamma(s,t)^* - \partial_t\gamma(s,t)^*\partial_s\gamma(s,t) = -2i \ . \tag{3.9}$$

Equation (3.9), plus the statement that $\partial_s\gamma(s,t)$ is analytic and nonzero whenever $s$ lies in the strip [Eq. (3.5c)], yields the evolution of the interface.

### C. An example

To show what all this means, we develop an example analogous to the stability analysis of Sec. I.B, but now specific to the zero-surface-tension case. We shall now get not just an expansion for small amplitudes, but an exact solution for the interface. To derive this, we replace the guesses [Eq. (1.8)] about the form of the pressure and the interface by a corresponding guess for $f_t(\Phi)$,

$$f_t(\Phi) = C_0(t) + \Phi/U + C_1(t)e^{-q\Phi/U} \ . \tag{3.10}$$

Here the first two terms would give a flat interface, while the third represents a "correction" with wave vector $q$. The actual interface is given by the curve traced out by $\gamma$ as a function of $s$, where

$$\gamma(s,t) = C_0(t) + is/U + C_1(t)e^{-isq/U} \ . \tag{3.11}$$

Notice that the nontrivial dependence upon $\Phi$ and $s$ is given in terms of

$$\omega = e^{-q\Phi/U} = e^{-isq/U} \ . \tag{3.12}$$

Our boundary conditions require that $C_0$ be real. Choose $C_1$ to be real also.

To see that Eq. (3.11) is an exact solution, simply differentiate and substitute into Eq. (3.9). The result is

$$(\dot{C}_0 + \omega\dot{C}_1)(1 - C_1q\omega^{-1}) + (\dot{C}_0 + \omega^{-1}\dot{C}_1)(1 - C_1q\omega) = 2U \ . \tag{3.13}$$

Equation (3.11) will be an exact solution if we can ensure that Eq. (3.13) is satisfied for all $s$. This will, in turn, be true if we can make the coefficients of $\omega^j$ for $j = 0, \pm 1$ each vanish. The resulting differential equations for $C_0$ and $C_1$ are

$$\frac{d}{dt}(2C_0 - C_1^2q) = 2U \ , \tag{3.14a}$$

$$\frac{d}{dt}\ln C_1 = C_0 \ . \tag{3.14b}$$

If $C_1 = 0$ at time zero, it remains zero. Then $C_0$ increases linearly in time, $C_0 = U(t - t_0)$, and, correspondingly, the interface moves forward with speed $U$. If, however, $C_1$ starts out positive but small, it will continually grow larger. The solution will remain acceptable until

$$\frac{\partial}{\partial s}\gamma(s,t) = \frac{i}{U}[1 - qC_1(t)\omega] \tag{3.14c}$$

vanishes at some $s$. This will happen at some finite time when $C_1$ becomes equal to $\pm q^{-1}$. At this time the interface acquires a cusp, and after that the evolution is not defined.

### D. Finger solution

There exist a few special solutions that do not go to cusps. One kind is the family of finger solutions found by Saffman and Taylor (1958). Here if the finger has a width $\lambda W$ and the fluid moves with speed $U$ at $x = +\infty$, then the speed at which the interface advances is $U/\lambda$. Thus as $\mathrm{Re}\Phi \to \infty$, we can expect a solution of the form

$$f_t(\Phi) = Ut/\lambda + \Phi/U + g(\Phi) \ , \tag{3.15a}$$

where $g$ vanishes rapidly as $\mathrm{Re}\Phi \to +\infty$. In order to construct a finger, we need a singularity as $\Phi$ goes to the corners of the strip, which lie at $\Phi = \pm iUW/2$. One guess is that there is a logarithmic singularity at these points, i.e., that

$$g(\Phi) = \alpha \ln(1 + e^{-2\pi\Phi/UW}) \ . \tag{3.15b}$$

Given this guess, one finds that

$$\frac{\partial}{\partial s}\gamma(s,t) = \frac{i}{U} - \frac{2\pi i\alpha}{WU}\frac{1}{1 + e^{2\pi is/(WU)}} \ . \tag{3.16}$$

Then, a brief calculation based upon Eq. (3.9) shows that Eq. (3.15a) is indeed a solution if

$$\alpha = \frac{W}{\pi}(1 - \lambda) \ . \tag{3.17}$$

This solution gives the profile described in Eq. (1.15), i.e., a single finger with width $\lambda$.

There are indeed other solutions of the form

$$f_t(\Phi) = Ut/\gamma + \Phi/U + \sum_{j=1}^{m} a_j \ln(e^{iq_j} + e^{-2\pi\Phi/UW}) \ , \tag{3.18}$$

with $a_j$ real and positive and $q_j$ real. These solutions have $m$ "channels" going off to $x \to -\infty$, and are thus a generalization of the original Saffman-Taylor solution [Eq. (3.15)]. These solutions are singular in the sense that the interface extends to infinity and the mapping has logarithmic singularities on the unit circle. The form of the steady-state solution given in Eq. (3.15) suggests the following ansatz for the time-dependent solutions:

$$f_t(\Phi)=\Phi/U+C_0(t)+\sum_{j=1}^{m} a_j \ln[\omega-p_j(t)] , \tag{3.19}$$

where $\omega$ is determined as a function of the complex potential $\Phi$,

$$\omega=e^{-2\pi\Phi/UW} . \tag{3.20}$$

The singularities of this map, $p_j(t)$, move with time but are confined outside the physical domain: $|p_j(t)|\geq 1$. When one of them hits the circle, a channel going to $x=-\infty$ is formed. We can write down the evolution equation for these singularities. It turns out, however, to be more convenient to track the zeros of $\partial_\Phi f$ instead. They must also lie outside the disk—otherwise the conformality requirement is not satisfied. We have

$$\partial_\Phi f=\alpha_0\frac{\prod_{j=1}^{m}[\omega-\alpha_j(t)]}{\prod_{j=1}^{m}[\omega-p_j(t)]} . \tag{3.21}$$

Proceeding along the lines developed by Shraiman and Bensimon (1984), and after some algebraic manipulations, one can obtain the "pole dynamics" equations: a system of $m$ ordinary differential equations governing the motion of the critical points of the map, $\alpha_j(t)$, of the form

$$\partial_t\alpha_j=F_j(\alpha,p) , \tag{3.22a}$$

$$\partial_t p_j=G_j(\alpha,p) . \tag{3.22b}$$

Note that, while the $p_j$'s completely determine the $\alpha_j$'s and vice versa [from Eqs. (3.19)—(3.21)], it is more convenient to track the evolution of zeros and poles by differential equations, since the relation involves high-order algebraic equations.

The simplest example is the case in which there is only one term in the sum in Eq. (3.19):

$$f_t(\Phi)=a_0(t)+\Phi/U+\frac{W}{2\pi}\ln[\omega-a_1(t)] . \tag{3.23}$$

Equations (3.22) then have the solution

$$\begin{aligned} a_0(t)&=2Ut , \\ a_1^2(t)&=1+[a_1^2(0)-1]e^{-2\pi tU/W} . \end{aligned} \tag{3.24}$$

In this case a cusp does not appear and, instead, the solution asymptotically approaches the Saffman-Taylor $\lambda=\frac{1}{2}$ steady-state solution.

The existence of a "pole" decomposition is somewhat surprising, since this is more commonly associated with integrable systems, such as, the Burgers equation (Calogero, 1975; Choodnovsky, 1977) and the $K\,dV$ equation (Kruskal, 1974; Moser, 1975), although it has been discovered in a few other systems as well (see Lee and Chen, 1982; Thual, Frish, and Henon, 1985).

The differential equations [Eqs. (3.22)] can be solved explicitly in some cases; otherwise, they can be studied numerically. It can be shown (Sarkar, 1984; Howison, 1985) that most initial conditions of the form of Eq. (3.21) lead to the appearance of $\frac{2}{3}$ power cusps on the interface when one of the zeros of $\partial_\Phi f$ hits the unit disk. Figure 10 shows an example of the appearance of such a cusp in the evolution of the initial interface given by

$$f(\Phi)=\Phi/U+\sum_{1}^{4}\ln[W-p_j(t)]+C_0(t) , \tag{3.25}$$

with $p(0)=(3,10i,-9i,-6+4i)$.

For most initial conditions, cusps form and, after they form, the equations seem to stop having solutions.

Physically, one expects the surface tension to prevent the singularities from appearing. Its effect should become important when the curvature near the cusp becomes of the order of the capillary length: $W\sqrt{d_0}$. It may be possible to understand this problem using the method of matched asymptotic expansions (see Bender and Orszag, 1978). However, this has not yet been done.

## IV. THE CONFORMAL MAPPING ALGORITHM

### A. Introduction

There are several different ways of studying the fluid flow that results when the surface tension is not zero. Some of them have already been mentioned. Section II outlined the application of random-walk techniques to this problem. Tryggvason and Aref (1983, 1986) have applied a method in which the interface is described as a vortex sheet, thereby constructing a set of very appealing simulations of time development. A slightly different boundary integral method was employed by DeGregoria and Schwartz (1986) in their simulations of interface evolution. Both groups found that apparently stable fingers are generated, at least for the not-too-small values of $d_0$ for which their calculations are accurate. Their fingers, in turn, look very much like the fingers that are obtained from a direct solution of the steady-state problem as set up by McLean and Saffman (1981).

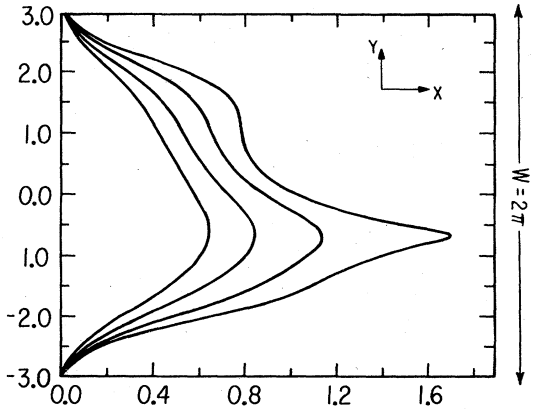


FIG. 10. Generation of a finite-time cusp in the evolution of an arbitrary initial interface in the absence of surface tension.

In this section we shall describe yet another method. This one is based upon the conformal mapping approach of Shraiman and Bensimon (1984) and was used in the simulations carried out by Bensimon (1986). Similar ideas were used by Menikoff and Zemach (1983) in simulating motion of interfaces. Our motivation for this particular focus is that this method seems particularly well suited to the study of the limit of small-surface tensions where the behavior remains a bit of a puzzle.

### B. Conformal method for the problem with surface tension

In Sec. III, the hodograph technique was used to derive the equation of motion of the interface. In this section we shall rederive this equation in the presence of surface tension ($d_0 \neq 0$) and from a slightly different approach. The velocity potential $\varphi$ obeys

$$\nabla^2 \varphi = 0 \tag{4.1a}$$

and the boundary conditions on the interface,

$$\varphi = \frac{Tb^2}{12\mu}\kappa \tag{4.1b}$$

and

$$\hat{\mathbf{n}}\cdot\nabla\varphi = \hat{\mathbf{n}}\frac{\partial \gamma}{\partial t} , \tag{4.1c}$$

where $\gamma$ is the interface between the two fluids, $\kappa$ its curvature, and $\hat{\mathbf{n}}$ a direction normal to the interface. Instead of including boundary conditions at the side walls, we assume here a periodicity under $y \to y + W$. This corresponds physically to a cylindrical Hele-Shaw cell such as the one used by Aribert (1970).

Equations (4.1) determine the evolution of the interface: the Laplace equation with the Dirichlet boundary condition on $\gamma$, Eq. (4.1b), completely determines the flow field; then, the value of the normal velocity (the normal gradient of $\varphi$) at the boundary determines the velocity of the interface, Eq. (4.1c). We have to solve a Stefan, or, moving-boundary-value problem. The two-dimensionality of the problem greatly simplifies the task by allowing the use of the conformal mapping technique.

The idea, which is standard in all textbooks on complex variables, e.g., Carrier, Krook, and Pearson (1966), is based on the Riemann mapping theorem. This theorem ensures the existence of a conformal map from the complicated, but simply connected, domain enclosed by the interface $\gamma$ into a standard domain, the interior of the unit disk. Within the disk the Dirichlet problem for the potential $\varphi$, Eqs. (4.1a) and (4.1b), can be readily solved. That solution then enables us to rewrite Eq. (4.1c) as an evolution equation for the mapping. As in Sec. III, we introduce the complex potential $\Phi(z) = \varphi(x,y) + \psi(x,y)$ (with $z = x + iy$). We then conformally map the domain of interest, i.e., the space occupied by the driven fluid, into the unit disk ($|\omega| \leq 1$): $z = f_t(\omega)$ (see Fig. 11). Since the interface $\gamma$ between the two fluids is the image

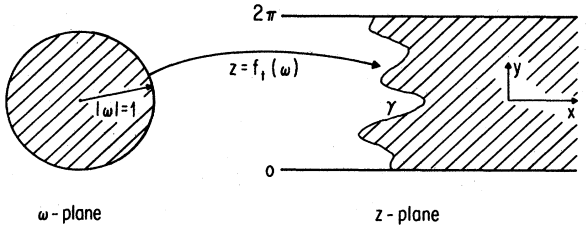


FIG. 11. Conformal map from the unit disk to the space occupied by the driven fluid.

of the unit circle ($|\omega| = 1$) under the map $f_t(\omega)$;

$$\gamma(t,s) = f_t(e^{is}) , \tag{4.2}$$

specifying the mapping $f_t(\omega)$, at a given time $t$, is identical to specifying the interface, $\gamma(t,s)$, together with its parametrization $s$.

In the unit disk, the solution of the Dirichlet problem is standard. One has to find the function analytic inside the unit disk, $\Phi(\omega)$, of which the real part on the boundary, $\omega = e^{is}$, is specified: $\varphi(s) = (Tb^2/12\mu)\kappa(s)$, where $\kappa(s)$, the local curvature of $\gamma(t,s)$, is

$$\kappa(s) = -\mathrm{Im}\frac{\partial_s^2 f / \partial_s f}{|\partial_s f|} . \tag{4.3}$$

The solution is known to be given by the Poisson integral formula. That formula states that the function analytic for $|\omega| < 1$, $\tilde{g}(\omega) = g(\omega) + ih(\omega)$, for which the real part on the unit disk $g(s)$ can be written as

$$g(s) = a_0 + \sum_{n=0}^{\infty} (a_n e^{ins} + a_n^* e^{-ins}) , \tag{4.4a}$$

must be

$$\tilde{g}(\omega) \equiv A\{g\}(\omega) = a_0 + 2\sum_{n=0}^{\infty} a_n \omega^n . \tag{4.4b}$$

Here, we interpret $A\{g\}$ as an integral operator applied to a real-valued function $g(s)$ defined on the unit circle, giving a complex-valued function $\tilde{g}(\omega)$ analytic within that circle.

This approach can be directly applied to the determination of the potential. First we deal with the trivial case in which we have a flat interface and the curvature vanishes. In this case the potential is $\Phi = Uz$, while the mapping that takes one from the unit disk $|\omega| \leq 1$ onto the strip $x > 0$, $-W/2 \leq y \leq W/2$ is $z = -(W/2\pi)\ln\omega$. Hence, in this example,

$$\Phi(\omega) = -\frac{UW}{2\pi}\ln\omega . \tag{4.5}$$

The singularity of $\Phi$ at $\omega = 0$ is simply a reflection of the $x \to \infty$ behavior of the problem. This behavior and this singularity will persist even in the presence of a nontrivial interface. Thus we can say that $\Phi(\omega) + (UW/2\pi)\ln\omega$ must be analytic for $|\omega| \leq 1$, and must have the value

given by Eq. (4.1b) on the circle. We use Eq. (4.4) to conclude that

$$\Phi(\omega)=-\frac{UW}{2\pi}\ln\omega+\frac{Tb^2}{12\mu}A\{\kappa\}(\omega)\ .$$

Following the notation of the theorem we use the notation $\tilde{\kappa}(\omega)$ for $A\{\kappa\}(\omega)$ and hence get an expression for the complex potential, which is

$$\Phi(\omega)=-\frac{UW}{2\pi}\ln\omega+\frac{Tb^2}{12\mu}\tilde{\kappa}(\omega)\ . \tag{4.6}$$

A comparison between Eqs. (3.20) and (4.6) will show that the $\omega$ used here will reduce to the $\omega$ of Sec. III as $T\to 0$. However, the $s$'s of the two sections are different. As $T\to 0$, the $s$ of this section is $-2\pi/UW$ times the $s$ of the preceding section.

Now, the normal velocity of the interface, given by Eq. (4.1c), is $(\hat{\mathbf{n}}\cdot\nabla)\varphi$, where $\hat{\mathbf{n}}$ is a unit vector normal to the interface. This vector can be rewritten in complex notation as

$$n=n_x+in_y=i\frac{\partial_s f}{|\partial_s f|}=-\frac{\omega\partial_\omega f}{|\omega\partial_\omega f|}\ . \tag{4.7a}$$

Here and in the rest of this section, $\omega$ is specified to lie on the unit circle. Given $n$ one can calculate the normal component of the gradient as

$$\begin{aligned}(\hat{\mathbf{n}}\cdot\nabla)\varphi&=n_x\partial_x\varphi+n_y\partial_y\varphi\\&=n_x\partial_x\varphi-n_y\partial_x\varphi\\&=\mathrm{Re}(n\partial_z\Phi)=\mathrm{Re}\left[n\frac{\partial_\omega\Phi}{\partial_\omega z}\right]\\&=-\frac{\mathrm{Re}(\omega\partial_\omega\Phi)}{|\omega\partial_\omega f|}\ .\end{aligned} \tag{4.7b}$$

Notice that Eq. (4.1c) only specifies the normal velocity of the interface. Of course there is no physical significance to a tangential velocity, which simply corresponds to a reparametrization of the interface.

However, the analyticity of the mapping function $f(\omega)$ fixes a particular "analytic," parametrization "gauge." This parametrization has to be maintained for all $t$. For that purpose, it is sufficient to make the time derivative of the map, $\partial_t f$, analytic inside the unit disk. To achieve this, as in Eq. (3.8), we add to the right-hand side of Eq. (4.6) an appropriate tangential velocity component,

$$\begin{aligned}\partial_t f&=n(\hat{\mathbf{n}}\cdot\nabla)\varphi+inC'\\&=\omega\partial_\omega f\left[\frac{\mathrm{Re}(\omega\partial\omega\Phi)}{|\omega\partial\omega f|^2}+iC\right].\end{aligned} \tag{4.8}$$

Here $C$ and $C'$ are real functions of $\omega$. To make the right-hand side of Eq. (4.9) analytic, the function $C$ has to be the harmonic conjugate of the first term in the large parentheses: $\mathrm{Re}(\omega\partial_\omega\Phi)/|\omega\partial_\omega f|^2$. In other words, the terms in the large parentheses have to represent the function analytic in $|\omega|\le 1$, the real part of which on $|\omega|=1$ is specified. We have seen previously that this is achieved by the Poisson integral formula as expressed in Eq. (4.4). Therefore, the use of Eqs. (4.4) and (4.6) upon Eq. (4.8) yields the desired evolution equation for the interface:

$$\frac{\partial f}{\partial t}=-\omega\partial_\omega f A\left[\frac{1-(d_0W/2\pi)\mathrm{Re}[\omega\partial_\omega\tilde{\kappa}(\omega)]}{|\omega\partial_\omega f|^2}\right]\frac{UW}{2\pi}\ . \tag{4.9}$$

### C. Numerical simulations

If we know $f_t(\omega)$ for a given value of $t$, we can obtain the entire right-hand side of Eq. (4.9) and thus find $\partial_t f$. This enables us to set up a numerical algorithm for simulating the evolution of $\gamma(s,t)$. This algorithm is rather efficient. One measure of its quality is the number of operations needed per time step. In this case, if one fits the interface at $N$ points and thus retains $N$ coefficients in a Fourier series like Eq. (4.4), then the computer code requires $O(N\ln N)$ operations per time step. (Most of the time is spent in computing Fourier series, using a fast Fourier transform algorithm.)

The algorithm was checked against known results in the asymptotic regime ($t\to\infty$). A typical outcome of such a simulation fits well the finger shape obtained by the phenomenological scaling hypothesis of Pitts (1980) [see Figs. 8 and 12(b)]. The dependence of the finger width on the McLean-Saffman surface-tension parameter $\kappa$ is shown in Fig. 7 and agrees with their numerical results for the steady-state interface. In the absence of surface tension, the time evolution of the interface was in complete agreement with the exact time-dependent solution. It developed finite-time singularities [see Figs. 10 and 12(a)]. In its presence, one observes two regimes. One is at low velocities ($d_0>10^{-2}$), for which an initial arbitrary interface evolves into the corresponding McLean-Saffman steady-state propagating finger [Fig. 12(b)]. The other is at high velocities ($d_0<10^{-2}$), for which the finger is unstable and shows wobbling and tip splitting [Fig. 12(c)]. This is in qualitative agreement with recent numerical and experimental work (Tabeling and Libchaber, 1986; Park and Homsy, 1985; Liang, 1986; DeGregoria and Schwartz, 1986). In Sec. V we shall use this algorithm to study the linear and nonlinear stability of the propagating finger.

## V. STABILITY OF THE FINGERS

### A. Anomalous stability

In Sec. I.C we discussed the difficulties associated with the stability analysis of the finger solutions. A naive argument given there suggested that since the capillary length $W\sqrt{d_0}$ is—for small $d_0$—small compared to the characteristic curvature of the finger, one might expect

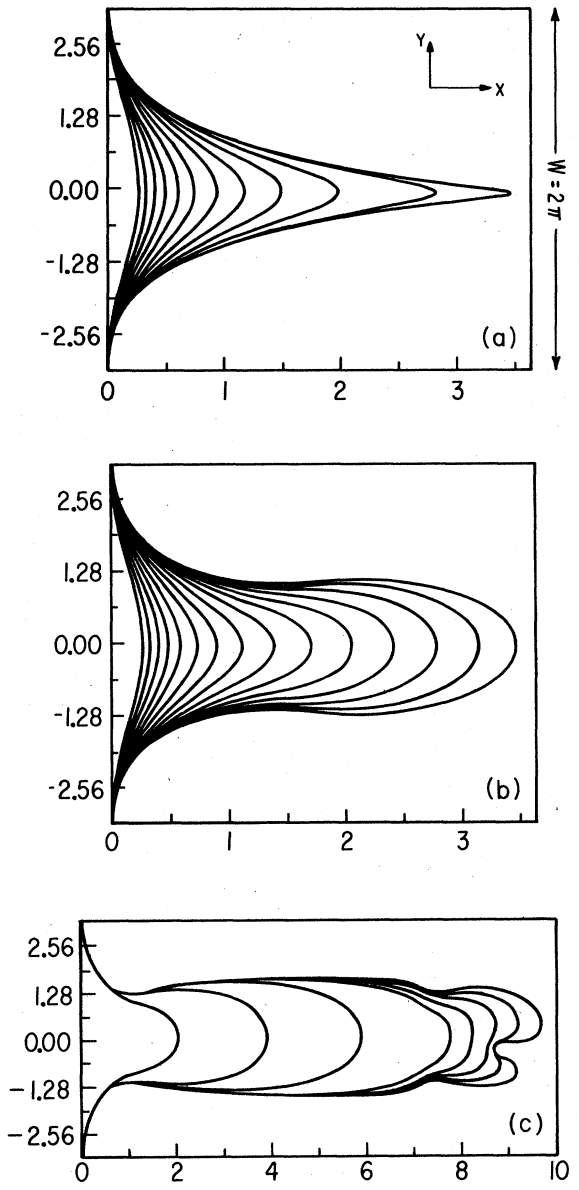


FIG. 12. Time evolution of an interface, from Bensimon (1986). Here the cell width $W$ is set equal to $2\pi$. The fluid moves to the right and successive interfaces are superposed on the same picture. (a) Evolution of an arbitrary initial interface without surface tension. (b) Evolution of the same initial interface as in (a), but in the presence of surface tension ($d_0=0.01$). (c) Tip splitting in the evolution of an interface at low surface tension ($d_0=0.01$).

the finger to be unstable just like the flat surface. This is, of course, at odds with experimental observations as well as numerical simulations. On the other hand, the direct linear stability analyses of Kessler and Levine (1986a, 1986b) and Bensimon (1986), carried out numerically, have shown the fingers to be stable to infinitesimal perturbation for all values of $d_0$. Kessler and Levine (1985b) suggested that the stability is due to the interaction with the walls of the cell.

A particularly illuminating observation was made by Tabeling and Libchaber (1986), who studied the behavior of the perturbed fingers in the real Hele-Shaw cell, and by DeGregoria and Schwartz (1986), who simulated the evolution of the fingers numerically. This observation was that the localized disturbance of the interface drifts along the finger onto its side, whereupon it slowly disappears.

The stabilization is thus due to the fact that the disturbance is expelled from the region of instability and does not have "enough time" to grow. This provides a valuable physical insight.[4]

As pointed out to us by Pelce, the physical mechanism involved is exactly the one proposed by Zel'dovich and co-workers (1980) to explain the stabilization of cellular flames. Below, we shall apply their ideas to the Saffman-Taylor problem. To verify the results obtained by the heuristic (and approximate) argument, we shall later in this section present the results of a more direct study of stability carried out by Bensimon (1986) using the complex analytic method outlined in Sec. III.

### B. Stability analysis in a WKB approximation

In this section we apply the ideas of Zel'dovich and coworkers (1980) to the Saffman-Taylor problem.[5] Consider a finger moving uniformly with velocity $U/\lambda$. Use as coordinates to describe this finger $\theta$, which is the angle between the normal to the interface and the $x$ axis, and $\tau$, the path length along the interface measured from the tip. On this interface superpose a small disturbance with amplitude $A$ and wave vector $q$ localized in some region described by $\tau$ or $\theta$. The amplitude is the height of the distortion measured perpendicular to the interface. For the localization idea to make any sense, the wavelength $2\pi/q$ must be very small in comparison to the typical dimension of the finger, $W/\lambda$. When this condition is satisfied we can consider $A$, $q$, and $\tau$ each to be functions of time $t$, or equivalently of $\theta$. (See Fig. 13.)

If we neglect the small effect of the disturbance, the velocity of the fluid normal to the surface is given by

$$v_n=\frac{U}{\lambda}\cos\theta\ . \tag{5.1a}$$

In the laboratory frame the velocity parallel to the interface is proportional to the gradient of the potential

[4]A similar mechanism was proposed by Landau and Lifshitz (1959) to explain the nonlinear instability occurring in Poiseuille flow.

[5]A related WKB scheme was used by Langer (1986) to obtain solutions for a model of solidification in the presence of surface tension, a singular perturbation.

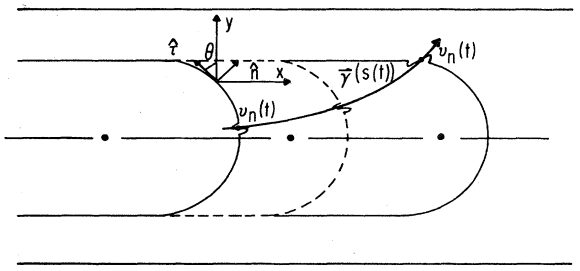


FIG. 13. Stretching and quenching of an initial localized perturbation of the finger.

along the interface, $(\partial_\tau \kappa)T$. In the fixed frame of the finger there is an additional term, the component of $U\hat{\mathbf{x}}$ parallel to the surface. We find that the component of the fluid velocity parallel to the surface is

$$U_\tau = \frac{U}{\lambda}\sin\theta - \frac{Tb^2}{12\mu}\partial_\tau \kappa \ . \tag{5.1b}$$

Assume that the disturbance propagates backward along the finger with the speed $U_\tau$. As it propagates it is stretched because $U_\tau$ varies in space. This stretching makes the wave vector change in time by

$$\frac{d}{dt}\ln q = -S \ , \tag{5.2}$$

where the stretching factor $S$ is given by

$$S = \frac{d}{d\tau}U_\tau \ . \tag{5.3}$$

The amplitude of the disturbance is also changed by the stretching. As the disturbance becomes wider it must be lower. Hence we get one term in $d_t \ln A$ which is just $-S$. Another term in the equation of motion for $A$ is that given in Eq. (1.13), in which

$$\frac{\dot{A}}{A} = q\left[\nu_n - \frac{Tb^2}{12\mu}q^2\right] .$$

Note that we use here the normal component of the velocity in determining the growth rate of the instability. When we put both effects together, we find

$$\frac{d}{dt}\ln A = q\left[\nu_n - \frac{Tb^2}{12\mu}q^2\right] - S \ . \tag{5.4}$$

Quadratures of these equations of motion can be obtained rather directly. Start from Eqs. (5.2) and (5.3) and use the fact that $d\tau = dt(d\tau/dt) = dtU_\tau$ to integrate and find that

$$q = C/U_\tau \ . \tag{5.5}$$

Here $C$ is a constant of integration. Since $U_\tau$ goes to zero at the tip, the wavelength goes to zero there. As $x \to -\infty$, $U_\tau$ becomes $U/\lambda$ so the wavelength approaches a constant at the base of the finger. Next we combine Eqs. (5.2) and (5.5) with the statement

$$dt = \frac{dt}{d\tau}\frac{d\tau}{d\theta}d\theta = \frac{1}{U_\tau \kappa}d\theta \ ,$$

to obtain

$$\frac{d}{d\theta}(\ln A - \ln q) = \frac{q}{U_\tau \kappa}\left[\nu_n - \frac{Tb^2}{12\mu}q^2\right] . \tag{5.6}$$

A solution can now be found by integrating with respect to $\theta$. We replace $q$ by $U$, making use of Eq. (5.5), and find

$$A(\theta) = \frac{A(\theta_0)U_\tau(\theta_0)}{U_\tau(\theta)}e^{I(\theta,\theta_0)} \ , \tag{5.7}$$

where the integral $I$ is

$$I(\theta_1,\theta_0) = \int_{\theta_0}^{\theta_1} d\theta \frac{C}{U_\tau^2 \kappa}\left[\nu_n - \frac{Tb^2}{12\mu}\frac{C^2}{U_\tau^2}\right] . \tag{5.8}$$

Equation (5.7) tells us about the amplification of the amplitude $A$ as the disturbance moves backward along the finger from $\theta_0$ to $\theta$. We shall be interested in estimating this amplification in the limit of small $d_0$, i.e., small-surface tension $T$. Notice that the integrand in Eq. (5.8) is fully defined once we specify the shape of the finger. That specification gives $\tau(\theta)$ and, hence, $\kappa = d\theta/d\tau$ as functions of $\theta$. From Eqs. (5.1) we then know $U_\tau$ and $\nu_n$. The integral can then, in principle, be done.

We are interested in understanding large amplifications. The largest possible amplification of $A$ times $U_\tau$ will occur if $\theta_0$ and $\theta_1$ are chosen to make the growth factor in the large parentheses of Eq. (5.8) exactly zero. The second term in the large parentheses is proportional to $T$ and hence is usually small. However, as $\theta$ goes to zero the tangential velocity $U_\tau$ also goes to zero. We estimate $U_\tau$ from the first term in Eq. (5.1b) and find that the large parentheses in Eq. (5.8) vanish for small $\theta$ when $\theta$ is equal to

$$\theta_0 = \left[\frac{Tb^2C^2}{12\mu(U/\lambda)^3}\right]^{1/2} . \tag{5.9}$$

As $\theta$ approaches $\pi/2$, $\nu_n$ goes to zero, and the stability factor can once again vanish, even though $T$ is small. This vanishing occurs at

$$\theta_1 = \pi/2 - \theta_0^2 \ . \tag{5.10}$$

The major contribution to the integral [Eq. (5.8)] occurs very near $\theta_0$, where the factor of $1/U_\tau^2$ produces a very large result. In this region, the disturbance is moving slowly, so that it has sufficient time to be amplified considerably. The result is that the integral takes on the value

$$I(\theta_1,\theta_0) \approx \frac{2C}{3\theta_0 \kappa_0 (U/\lambda)} \ . \tag{5.11}$$

Here $\kappa_0$ is the value of the curvature near the tip. From

the Saffman-Taylor $\lambda=\frac{1}{2}$ solution, we have $\kappa_0=2\pi/W$. We then find

$$I(\theta_1,\theta_0)=\frac{2^{3/2}}{3}\frac{1}{\sqrt{d_0}} . \tag{5.12}$$

All along we have tacitly assumed that the amplitude of the distortion remains small compared to the characteristic length $W$ of the finger. If the initial disturbance is weak enough, its amplitude is guaranteed to remain bounded and small by Eq. (5.11). However, larger disturbances, those leading to $A_{\max}\sim W$, are dangerous and may cause an instability. This suggests an estimate for the threshold of the finite-amplitude instability:

$$A_c\sim We^{-0.94d_0^{-1/2}} . \tag{5.13}$$

Here we neglect the subleading corrections given by the $U_\tau$ factors in Eq. (5.7).

The physical mechanism described above provides an explanation for the result of the linear stability analysis. It also provides an estimate for the order of magnitude (and $d_0$ dependence) of the threshold of the finite-amplitude instability.

The main limitation of the method used in this section is the need to assume that the length scale of the distortion is small compared to the local radius of curvature, so that the result for the stability of flat interfaces could be used. This restricts its applicability to the study of short-wavelength, localized distortions. Thus the analysis of this section does not replace the direct stability analysis, which will be discussed next.

### C. Stability analysis: the complex analytic method

The complex method can be directly used to study the stability of a steadily propagating finger. The method is directly analogous to that used in Sec. I.B. Assume that the conformal map describing the moving interface is

$$f_t(\omega)=f^0(\omega)+A_t(\omega) . \tag{5.14}$$

Here $f^0(\omega)$ is the steady-state finger solution, which then depends upon $d_0$, and $A_t(\omega)$ is a small time-dependent deviation from this solution. Since $f_t(\omega)$ is analytic inside the unit disk, we may assume

$$\begin{aligned} f^0(\omega)&=\sum_{n=0}^{\infty} f_n\omega^n , \\ A_t(\omega)&=\sum_{n=0}^{\infty} A_n(t)\omega^n . \end{aligned} \tag{5.15}$$

The stability analysis is performed by expanding Eq. (4.9) and keeping terms of first order in $A$.

Since $f^0$ is a steady-state solution, the result is an equation of the form

$$\dot{A}_k(t)=\sum_{n=1}^{\infty} M_{kn}[f^0]A_n(t)+M'_{kn}[f^0]A_n^*(t) . \tag{5.16}$$

Notice that the matrices $M$ and $M'$ depend upon the presumed steady-state solution $f^0$. The $k=0$ term in Eq. (5.16) gives $\partial_t A_0=0$, thus yielding a marginal mode that corresponds to the translation of the finger. The fact that it decouples from the rest is quite convenient and is an advantage of the method.

The solution to the linear stability problem can now be clearly seen. Consider $M$ and $M'$ in Eq. (5.16) to be matrices. Form the supermatrix

$$M=\begin{bmatrix} M & M' \\ M'^* & M^* \end{bmatrix} . \tag{5.17}$$

If that matrix has an eigenvalue $E$, then $A_n(t)$ is exponential in $t$, $e^{Et}$. Stability then requires that the real part of the eigenvalue be negative, so that any deviation from the finger solution would vanish as $t\to\infty$.

Once the matrix elements are written down, the eigenvalues can be calculated numerically. Bensimon (1986) expanded $f^0$ in a power series in $d_0$ and then used that expansion to calculate $M$ and $M'$ to first order in $d_0$. The eigenspectrum for $d_0=0.05$ is shown in Fig. 14. Notice the continuum of symmetric modes ($A_n$ real) and antisymmetric modes ($A_n$ imaginary) with a negative real eigenvalue preceded by a discrete set of asymmetric modes with complex eigenvalues (their number increases as $d_0\to 0$). The eigenvalues all have negative real parts for values of $d_0$ down to $10^{-3}$, so that the interface appears to be linearly stable. This is in agreement with the heuristic argument described in Sec. V.B. This stability result, as well as the eigenvalue spectrum, is also in agreement with previous results of Kessler and Levine (1985b). It disagrees with the results of McLean and Saffman (1981), where instability was predicted. However, Sarkar has argued that the instability prediction might be wrong because of neglected terms of order $d_0$, while Levine suggested that the number of mesh points was not sufficient to ensure accuracy. It appears to us that the results of Kessler and Levine (1985b) and Bensimon (1986) are the most reliable.

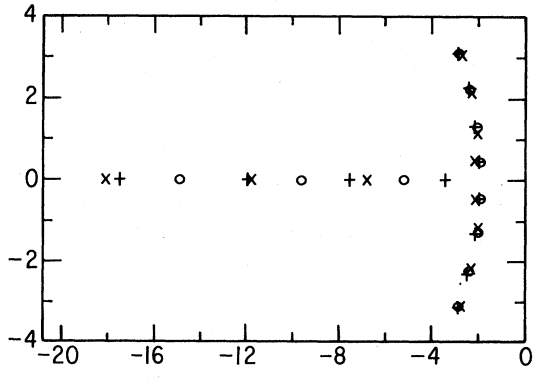


FIG. 14. Eigenspectrum at $d_0=0.05$, for various truncations of Eq. (5.16): +, $N=130$; ○, $N=100$; ×, $N=80$. Notice the discrete spectrum of asymmetric modes (complex eigenvalues) and the continuum of symmetric and antisymmetric modes (negative real eigenvalues). From Bensimon (1986).

### D. Structural stability and nonlinear instability

We have seen that the finger is destabilized due to the existence of a finite-amplitude instability. Its proximity shows up as a sensitivity of the eigenspectrum of the linearized problem. Bensimon (1986) argued that there is a relation between the structural stability of the linearized problem and the nonlinear instability of the full problem.

One may study the dependence of the critical amplitude for destabilization on $d_0$ by looking at the appearance of unstable modes in response to a random distortion of the interface [letting the $f_m$ in Eq. (5.15) contain a random term], an instability arising at a typical perturbation strength $v_c$ that depends upon $d_0$. For example, we can obtain a fit with a form

$$v_c \sim d_0^{1/2} \exp(-\beta d_0^{-1/2}) , \tag{5.18}$$

with $\beta \approx 1.3$. This particular form for the fit was suggested by the argument of Sec. V.B [Eq. (5.13)]. However, one should not necessarily expect full agreement between $v_c$ and the $A_c$ of Eq. (5.13). They are different quantities, although they are probably asymptotically equal. Other fits are possible—for example, $v_c \approx \exp(-\gamma d_0^{-\beta})$, with $\beta \approx 0.61$ and $\gamma \approx 0.72$. They all exhibit a singular behavior as $d_0 \to 0$.

When the noise in $f^0$ is larger than $v_c$, unstable modes arise. The most unstable modes are shown in Fig. 15: There are two asymmetric oscillatory modes, which we call the "hump" and "tip-wobbling" modes, and a symmetric nonoscillatory one that correspond to a change in the width $\lambda$ of the finger. These modes have apparently been observed in numerical simulations [Fig. 9(a); Liang, 1986] and in experiments (Tabeling and Libchaber, 1986).

The conjecture that the structural stability of the spectral problem is related to a finite-amplitude instability was verified numerically with the help of the algorithm based on the conformal mapping technique described in Sec. IV. This was done by studying the threshold of the instability at a given value of $d_0$ as a function of the amplitude of an initial random analytic perturbation of the

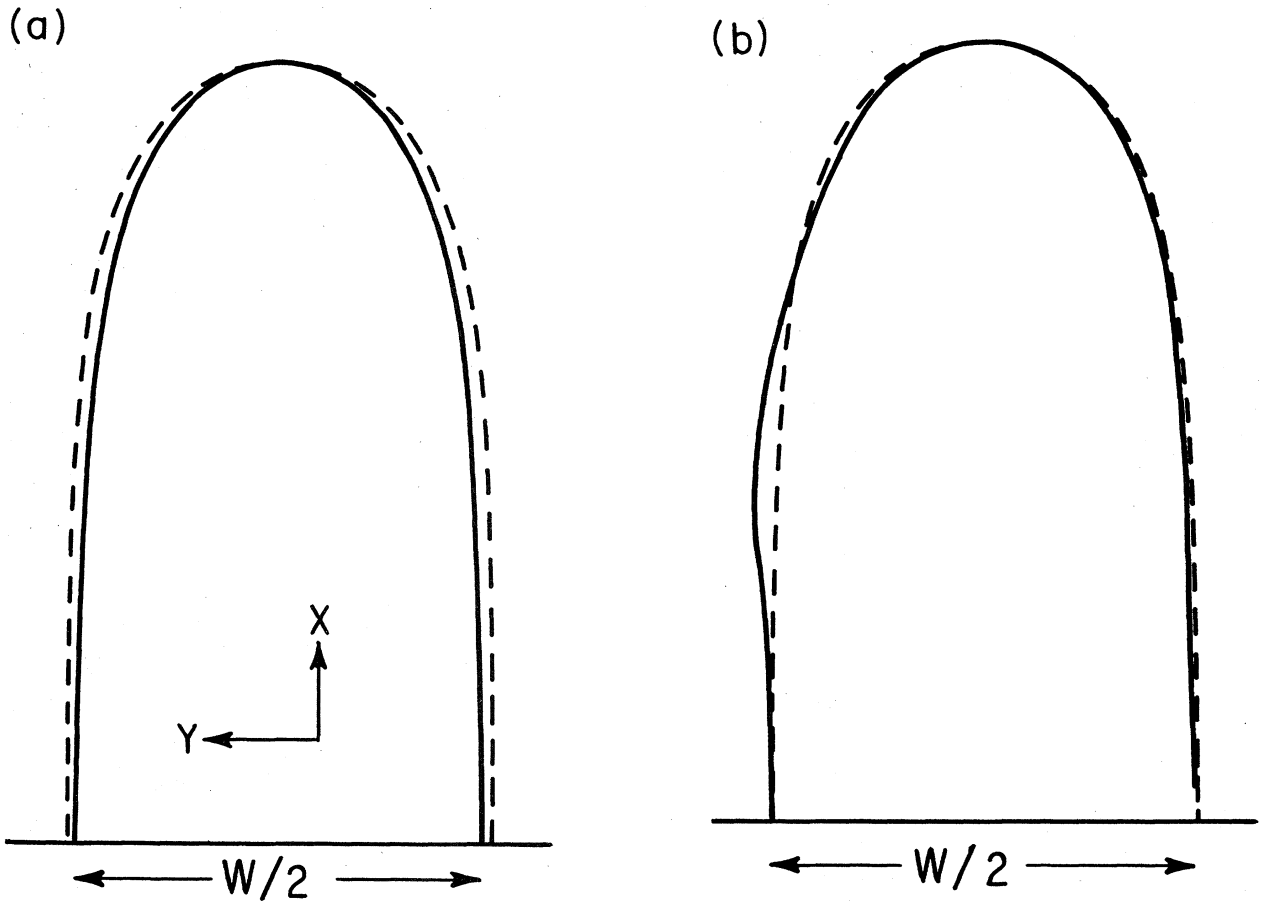


FIG. 15. The three least stable modes of the $\lambda = \frac{1}{2}$ finger (dashed line, unperturbed finger). (a) Symmetric nonoscillatory mode, which may be responsible for the experimentally and numerically observed fingers of width $\lambda < \frac{1}{2}$. (b) Asymmetric "hump" mode. (c) Asymmetric "tip-wobbling" mode. (d) Asymmetric "hump" mode observed in an experiment [courtesy of Tabeling and Libchaber (1986)].

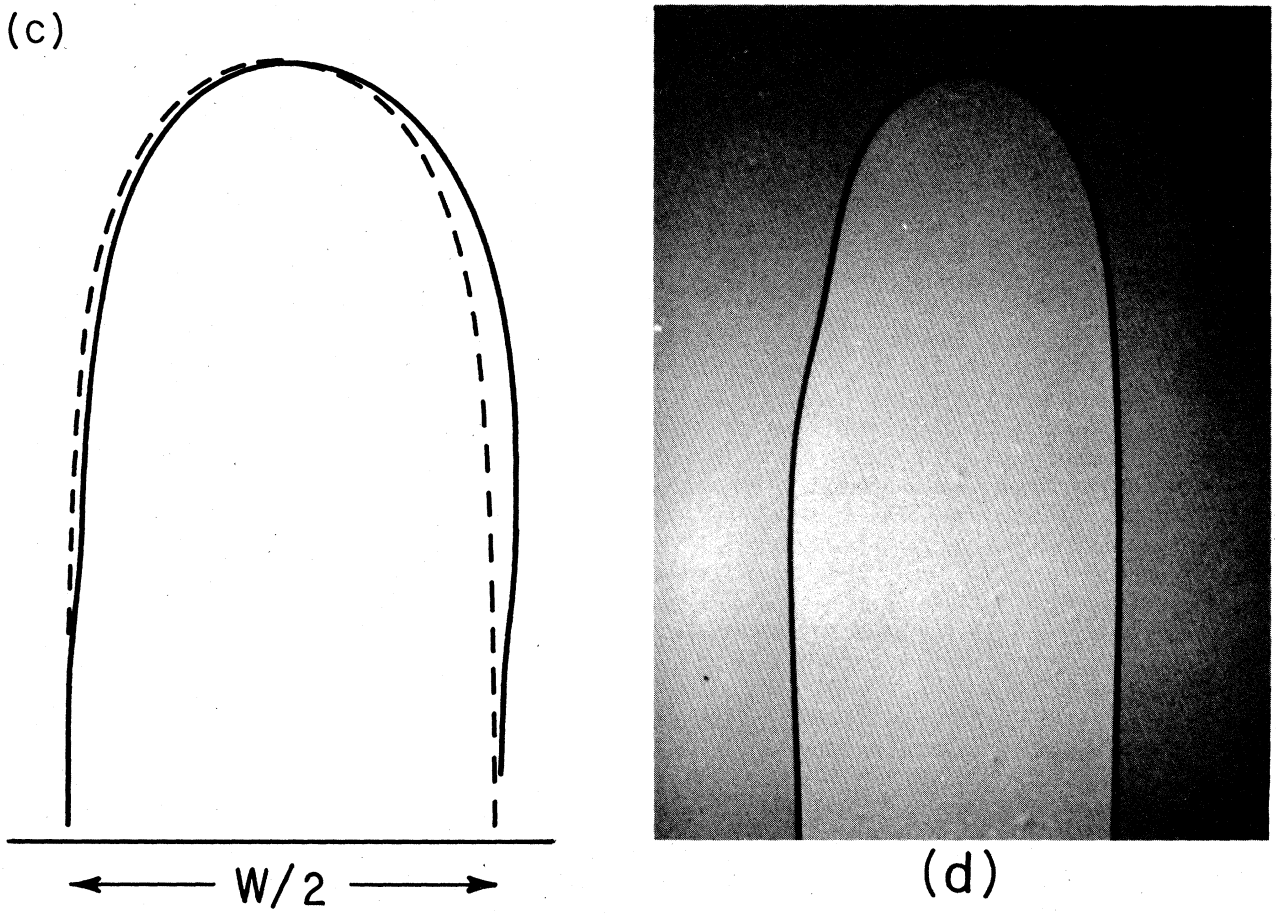


FIG. 15. (*Continued*).

interface. Figure 16 compares the results of the structural stability analysis and the numerical simulations. This comparison confirms the existence of a finite-amplitude instability whose threshold depends singularly on $d_0$, possibly of the form predicted by Eq. (5.13).

## CONCLUSION

Although the problem of the stability of the $\lambda=\frac{1}{2}$ Saffman-Taylor finger seems to be understood from different theoretical, numerical, and experimental approaches, one major question remains as yet unanswered. That is the question of selection, which is common to many related problems (solidification, dendritic growth, etc.). We do not yet understand the physical mechanisms at work behind the selection of one particular state out of a continuous—or discrete—family of possible solutions. Noise probably plays an important role via some destabilization scheme similar to that discussed in Sec. V.

Another (related?) scenario is that of dynamical selec-

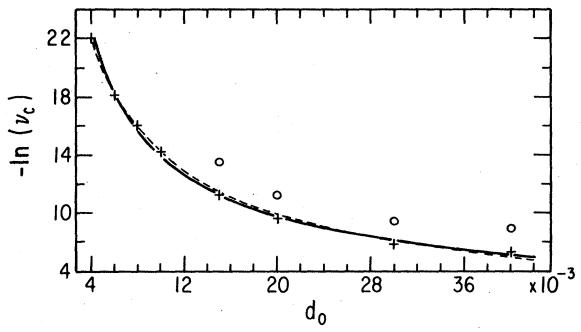


FIG. 16. Critical noise amplitude $\nu_c$ necessary to drive the system unstable as a function of the surface-tension parameter $d_0$. Notice that the vertical scale is logarithmic (we plot $-\ln\nu_c$ vs $d_0$): +, results of the structural stability analysis; solid curve, best fit of the form $\nu_c=\exp(-\gamma d_0^{-\beta})$ with $\beta=0.61$ and $\gamma=0.72$; dashed curve, best fit of the form $\nu_c\sim d_0^{1/2}\exp(-\alpha d_0^{-1/2})$ with $\alpha=1.3$; ○, results of the numerical simulations, which seemed to be more sensitive to noise by a constant factor. From Bensimon (1986).

tion. All possible solutions are linearly stable, but the selected one has a larger basin of attraction, thereby attracting all physically accessible initial states. Such a scenario is known to occur in one-dimensional, nonlinear diffusion equations (Kolmogorov *et al.*, 1937; Fisher, 1937; Aronson and Weinberger, 1978) and in a class of nonlinear first-order partial differential equations (Shraiman and Bensimon, 1985). Clearly an understanding of the transient regime where surface tension is dynamically important—preventing the formation of a cusp—is needed.

Despite these unanswered questions, many of the major aspects of viscous flows in Hele-Shaw cells are now reasonably well understood. We know that in a noise-free environment a single stable finger will eventually arise whenever the surface tension is nonzero. We understand that a small-surface tension is a singular perturbation that produces results qualitatively different from the integrable but unstable behavior at zero-surface tension. The instability of fingers against small amounts of noise at low-surface tensions is semiquantitatively understood. Calculations have been done that show in detail the role of the singular perturbation in producing the selected pattern. The discrepancy between theory and experiment in the observed values of the finger width $\lambda W$ as a function of the surface-tension parameter $d_0$ is apparently a result of the wetting of the glass plates.

One might expect this complex of ideas, and especially the idea of a singular perturbation, to be an important part of our understanding of other free interface problems. Rapid progress is being achieved in describing directional solidification, electrodeposition, and so forth. In the next few years considerable progress is to be expected in these problems of dynamical pattern formation. In fact, it might be that several features of these problems will emerge as the result of different kinds of singular perturbations upon the basic zero-tension Saffman-Taylor problem.

## ACKNOWLEDGMENTS

The research reported here was supported by the DOE, ONR, NSF, and the University of Chicago's Materials Research Laboratory. Every step of the work was aided by a lively interchange with the experimental group of F. Heslot, A. Libchaber, and P. Tabeling. At several points S. Sarkar joined us in our work. In addition, we have been helped by a frank and timely interchange of views and data with many of the other workers in the field, including H. Aref, E. Ben-Jacob, A. DeGregoria, F. Family, U. Frisch, N. Goldenfeld, S. Howison, J. Kertesz, D. Kessler, J. Koplik, J. Langer, R. Lenormand, H. Levine, J. Nittman, P. Pelce, Y. Pomeau, P. Saffman, L. Schwartz, G. Tryggvason, T. Vicsek, and T. Witten. Work in this area has been made much more pleasant by the vigorous exchanges mentioned above.

## REFERENCES

Aribert, J.-M., 1970, Ph.D thesis (Toulouse).
Aronson, D. G., and H. F. Weinberger, 1978, Adv. Math. **30**, 33.
Barenblatt, G. I., 1979, *Similarity, Self Similarity and Intermediate Asymptotics* (Consultants Bureau, New York).
Barenblatt, G. I., and Ya. B. Zel'dovich, 1972, Annu. Rev. Fluid Mech. **4**, 285.
Bender, C. M., and S. A. Orszag, 1978, *Advanced Mathematical Methods for Scientists and Engineers* (McGraw-Hill, New York).
Ben-Jacob, E., N. Goldenfeld, G. Kotliar, and J. Langer, 1984, Phys. Rev. Lett. **53**, 2110.
Bensimon, D., 1986, Phys. Rev. A **33**, 1302.
Birkhoff, G., and E. Zarantonello, 1957, *Jets, Wakes and Cavities* (Academic, New York).
Calogero, F., 1975, Lett. Nuovo Cimento **13**, 411.
Carrier, G. F., M. Krook, and C. E. Pearson, 1966, *Function of Complex Variable* (McGraw-Hill, New York).
Choodnovsky, D. V., and G. V. Choodnovsky, 1977, Nuovo Cimento B **40**, 339.
Chuoke, R. L., P. van Meurs, and C. van der Poel, 1959, Pet. Trans. AIME **216**, 188.
DeGregoria, A. J., and L. W. Schwartz, 1986, J. Fluid Mech. **164**, 383.
DiBenedetto, E., and A. Friedman, 1984, Trans. Am. Math. Soc. **282**, 183.
Elliot, C. M., and V. Janovsky, 1981, Proc. R. Soc. Edinburgh, Sect. A **88**, 93.
Fisher, R. A., 1937, Ann. Eugen. **7**, 355.
Hele-Shaw, H. J. S., 1898, Nature (London) **58**, 34.
Howison, S. D., 1985, SIAM Appl. Math. **46**, 20.
Howison, S. D., T. R. Ockendon, and A. A. Lacey, 1985, Q. J. Mech. Appl. Math. **38**, 343.
Kadanoff, L. P., 1985, J. Stat. Phys. **39**, 267.
Kessler, D. A., J. Koplik, and H. Levine, 1984, Phys. Rev. A **30**, 3161.
Kessler, D. A. and H. Levine, 1985a, Proceedings of the Electrochemical Society of America, Toronto, unpublished.
Kessler, D. A., and H. Levine, 1985b, Phys. Rev. A **32**, 1930.
Kessler, D. A., and H. Levine, 1986a, Phys. Rev. A **33**, 2621.
Kessler, D. A., and H. Levine, 1986b, Phys. Rev. A **33**, 2634.
Kolmogorov, A. N., I. G. Petrovsky, and N. S. Piskunov, 1937, Bull. Mosk. Univ. Ser. **A1**, No. 6.
Kruskal, M. D., 1974, in *Nonlinear Wave Motion,* edited by A. Newell (American Mathematical Society, Providence), p. 61.
Landau, L. D., and E. M. Lifshitz, 1959, in *Fluid Mechanics* (Pergamon, Oxford).
Langer, J. S., 1986, Phys. Rev. A **33**, 435.
Lee, Y. C., and H. H. Chen, 1982, Phys. Scr. **T2**, 41.
Liang, S., 1986, Phys. Rev. A **33**, 2663.
Maher, J., 1985, Phys. Rev. Lett. **54**, 1498.
McLean, J. W., 1980, Ph.D. thesis (California Institute of Technology).
McLean, J. W., and P. G. Saffman, 1981, J. Fluid Mech. **102**, 455.
Meiron, D., 1986, Phys. Rev. A **33**, 2704.
Menikoff, R., and C. Zemach, 1983, J. Comput. Phys. **51**, 28.
Meyer, G. H., 1982, in *Numerical Treatment of Free Boundary Value Problem,* edited by J. Albrecht (Birkhauser, Basel), p. 202.
Moser, J., 1975, Adv. Math. **16**, 197.

Nittmann, J., G. Daccord, and H. E. Stanley, 1985, Nature (London), Phys. Sci. **314**, 141.
Park, C.-W., and G. M. Homsy, 1984, J. Fluid Mech. **139**, 291.
Park, C.-W., and G. M. Homsy, 1985, Phys. Fluids **28**, 1583.
Paterson, L., 1984, Phys. Rev. Lett. **52**, 1621.
Pelcé, P., and Y. Pomeau, 1986a, Stud. Appl. Math. **74**, 245.
Pelcé, P., 1986b, thesis, University of Provence.
Pietronero, L., and H. J. Wiesmann, 1984, J. Stat. Phys. **36**, 909.
Pitts, E., 1980, J. Fluid Mech. **97**, 53.
Richardson, S., 1972, J. Fluid Mech. **56**, 609.
Saffman, P. G., and G. I. Taylor, 1958, Proc. R. Soc. London, Ser. A **245**, 312.
Sarkar, S., 1984, Phys. Rev. A **31**, 3468.
Shraiman, B. I., and D. Bensimon, 1984, Phys. Rev. A **30**, 2840.
Shraiman, B. I., and D. Bensimon, 1985, Phys. Scr. **T9**, 123.
Szép, J., J. Cserti, and J. Kertész, 1985, J. Phys. A **18**, L413.
Tabeling, P., and A. Libchaber, 1986, Phys. Rev. A **33**, 794.
Tang, C., 1985, Phys. Rev. A **31**, 1977.
Thual, O., U. Frish, and M. Henon, 1985, Nice Observatory report, unpublished.
Tryggvason, G., and H. Aref, 1983, J. Fluid Mech. **136**, 1.
Tryggvason, G., and H. Aref, 1986, J. Fluid Mech. **154**, 287.
Vanden-Broeck, J.-M., 1983, Phys. Fluids **26**, 2033.
Vicsek, T., 1984, Phys. Rev. Lett. **53**, 2281.
Witten, T. A., and L. M. Sander, 1981, Phys. Rev. Lett. **47**, 1400.
Witten, T. A., and L. M. Sander, 1983, Phys. Rev. B **27**, 5686.
Zel'dovich, Ya. B., A. G. Istratov, N. I. Kidin, and V. B. Librovitch, 1980, Combust. Sci. Technol. **24**, 1.
Zocchi, G., P. Tabeling, and A. Libchaber, 1986, J. Fluid Mech., to be published.

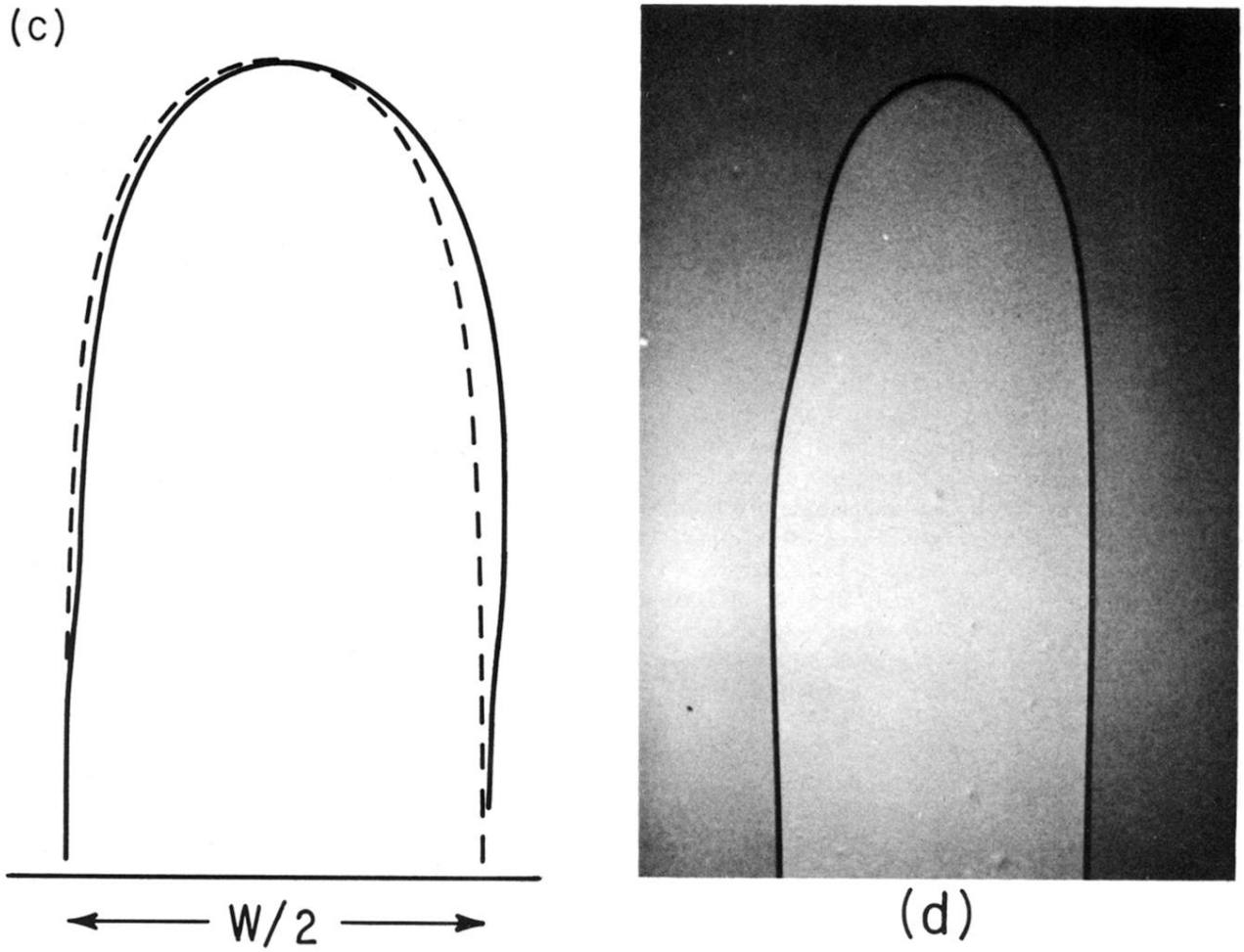


FIG. 15. (*Continued*).

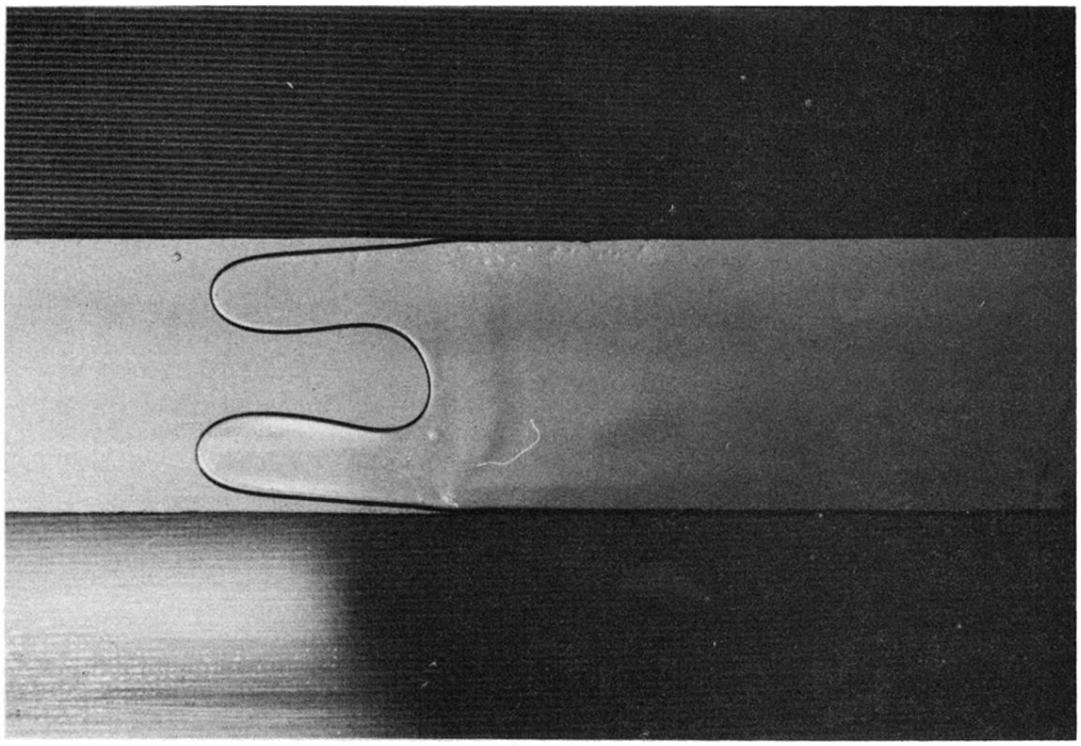

(a)

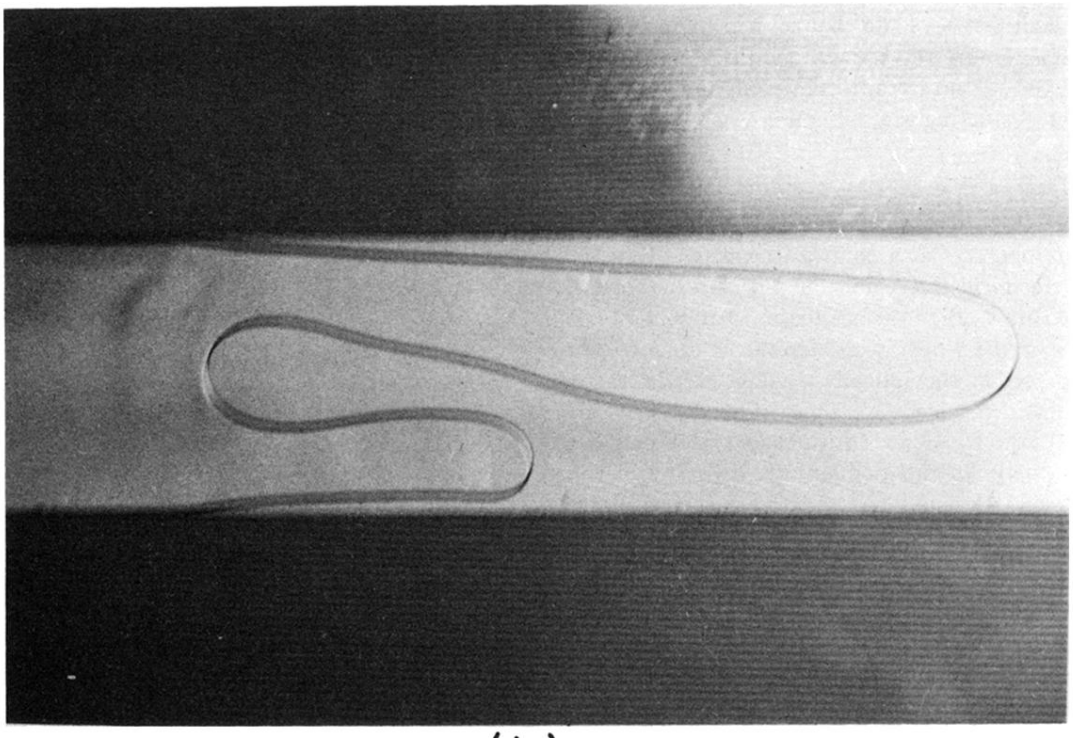

(b)

FIG. 2. Competition between two bumps leading to the emergence of a single propagating finger, courtesy of Tabeling and Libchaber (1986). Parts (a), (b), and (c) represent successively later times in the development of the same run.

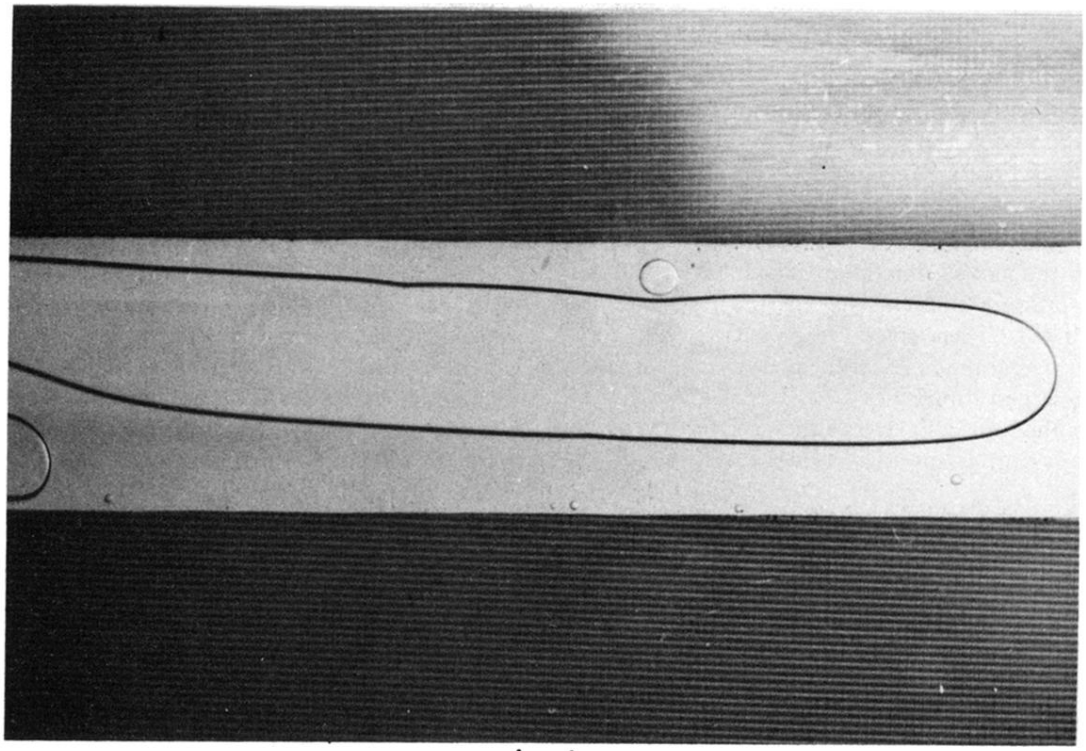


FIG. 2. (*Continued*).